A review of all-vanadium redox flow battery durability: degradation mechanisms and mitigation strategies

Yuan, Xiao-Zi; Song, Chaojie; Zhao, Nano; Platt, Alison; Li, Hui; Wang, Haijiang; Fatih, Khalid; Jang, Darren

https://doi.org/10.4224/40002765

Report (National Research Council Canada. Energy, Mining and Environment); no. NRC-EME-55984, 2018-12-05

NRC·CNRC

A Review of All-Vanadium Redox Flow Battery Durability: Degradation Mechanisms and Mitigation Strategies

Report No.: NRC-EME-55984
Date: December 05, 2018

Authors: Xiao-Zi Yuan*, Chaojie Song*, Nana Zhao, Alison Platt, Hui Li#, Haijiang Wang#, Khalid Fatih, Darren Jang

Energy, Mining & Environment Research Centre
National Research Council Canada
4250 Wesbrook Mall, Vancouver, BC, V6T 1E5, Canada

South University of Science and Technology of China
1088 Xueyuan Blvd, Nanshan District
Shenzhen, Guangdong 518055, China

*Corresponding authors:
Xia-Zi Yuan: xiao-zi.yuan@nrc.gc.ca; 1-604-221-3000 ext. 5576
Chaojie Song: chaojie.song@nrc.gc.ca; 1-604-221-3000 ext. 5577

National Research Council Canada | Conseil national de recherches Canada

Canada

Paper: Cat. No. NR16-248/2018E
ISBN 978-0-660-28844-4

PDF: Cat. No. NR16-248/2018E-PDF
ISBN 978-0-660-28843-7

Abstract

The all-vanadium redox flow battery (VRFB) is emerging as a promising technology for large scale energy storage systems due to its scalability and flexibility, high round-trip efficiency, long durability, and little environmental impact. As the degradation rate of the VRFB components is relatively low, less attention has been paid in terms of VRFB durability in comparison with studies on performance improvement and cost reduction. This paper reviews publications on performance degradation mechanisms and mitigation strategies for VRFBs in an attempt to achieve a systematic understanding of VRFB durability. Durability studies of individual VRFB components, including electrolyte, membrane, electrode, and bipolar plate are introduced. Various degradation mechanisms at both cell and component levels are examined. Following these, applicable strategies for mitigating degradation of each component are compiled. In addition, this paper summarizes various diagnostic tools to evaluate component degradation, followed by accelerated stress tests and models for aging prediction that can help reduce the duration and cost associated with real lifetime tests. Finally, future research areas on the degradation and accelerated lifetime testing for VRFBs are proposed.

Keywords: Redox flow battery; vanadium redox flow battery; durability; degradation; mitigation; diagnostic tools.

Highlights:

- Components and their durability studies of a VRFB are introduced.
- Various degradation mechanisms at both cell and component levels are examined.
- Applicable mitigation strategies for alleviating degradation are compiled.
- Accelerated stress tests and models for aging prediction are collected.
- Future research directions on VRFB degradation and mitigation are pointed out.

Table of Contents

1. Introduction

Renewable resources, such as solar, wind and hydropower, are increasingly being utilized due to the depletion of fossil fuels and anthropogenic climate change. As these resources are usually unpredictable, there is an imperative need for grid-connected energy storage systems to complement and employ renewable energies [1]. Electrochemical storage systems, such as sodium sulfur batteries, lithium-ion batteries, redox flow batteries (RFBs), and lead acid batteries [2], offer a solution because of their flexibility, efficiency, scalability, and other appealing features. By comparing the technicalities of different energy storage devices [3], the functional capabilities and technical advantages of RFBs are well suited to meet many of the demands for large-scale grid storage.

1.1. Redox flow batteries (RFBs)

In 1971, the polarization characteristics of a redox-type fuel cell was first studied by Ashimura and Miyake using a flow-through porous carbon electrode. In 1973, NASA (National Aeronautics and Space Administration, U.S.A.) founded the Lewis Research Center at Cleveland and started researching electrically rechargeable redox flow cells [4]. They investigated the fundamental feasibility of the overall redox concept, screened candidate redox couples to achieve optimum cell performance, and conducted system analysis and modeling to estimate costs [5][6]. Since then, significant progresses on RFB chemistries, materials, and systems has been made globally.

RFBs have been gaining momentum in both research and industry due to their relatively low capital and cycle cost in comparison with other energy storage technologies [3] and their ability to efficiently store large amounts of electrical energy in a world of expanding renewable energy. The most appealing features of this technology are: scalability and flexibility, independent sizing of power and energy, high round-trip efficiency, long cycling and calendar lifetimes, rapid response to load changes, reasonable capital costs, tolerance to deep discharges, and reduced environmental impact [7]. Theoretically, the primary drawback of a redox system is its high-volume due to the low energy density of the reactant solutions, reflected in costs for land and tankage [8].

In the traditional sense, redox systems are not batteries; they have a much greater similarity to fuel cell systems. They can be classified by active species or by solvent (aqueous and non-aqueous, respectively). Based on the active species, important RFB types include iron/chromium [4], bromine/polysulfide [9], all-vanadium [10], vanadium/bromine [11], zinc/bromine [12], and other configurations [13][14], each having its advantages, disadvantages, and challenges. Various types of flow batteries are summarized by Ulaganathan et al. [15] and performance characteristics are also quantitatively compared. There have been comprehensive and critical reviews of the features of this type of battery, focusing on the RFB chemistry, systematic classification, current status, recent progresses, and challenges [16][17][18][19].

A generic RFB cell consists of an anolyte (negative electrolyte), porous electrodes, a catholyte (positive electrolyte), and a separator (typically an ion-exchange membrane to separate the anolyte and catholyte solutions). The general reactions can be written as [1]:

During charge:

$$\text{Anode: } B^{m+} - ye^- \xrightarrow{charge} B^{(m+y)+} \quad (1)$$

$$\text{Cathode: } A^{n+} + xe^- \xrightarrow{charge} A^{(n-x)+} \quad (2)$$

During discharge:

$$\text{Anode: } A^{(n-x)+} \xrightarrow{discharge} A^{n+} + xe^- \quad (3)$$

Cathode: $B^{(m+y)+} \xrightarrow{discharge} B^{m+} - ye^{-}$ (4)

The principle of a RFB cell is a pair of electrochemical reduction and oxidation reactions occurring within two liquid electrolytes containing metal ions [20]. As the cell charges, the oxidation half reaction occurs on the anode, and electrons are released; on the cathode, the reduction half reaction occurs by receiving electrons, and ions migrate through a polymer electrolyte membrane to maintain electric neutrality. Both half-cells are connected to external storage tanks providing the needed volume of electrolyte circulated by pumps.

1.2. All-vanadium redox flow batteries (VRFBs)

Although various flow batteries have been undergoing development for the last 30 years, the all-vanadium redox battery (VRFB) has been found most appealing because both the anolyte and catholyte employ the same element, avoiding cross-contamination of the two half-cell electrolytes. VRFBs have become the most promising and commercially exploited RFB type for storing intermittent renewable energy [21].

A typical VRFB energy storage system is shown in Figure 1 (a), which principally consists of two key parts: the cell stacks, where chemical energy and electricity are converted in reversible processes, and the tanks, where electrolytes are stored [22]. Basically, the VRFB stack is similar to a proton exchange membrane (PEM) fuel cell stack and a single VRFB cell is similar to a PEM fuel cell, as presented in Figure 1 (b) [23].

In some configurations, not only the structure of a VRFB stack or a single cell, but also the membrane electrode assembly are similar to those of a PEM fuel cell. The materials used can also be similar in some cases. Ion exchange membranes used are typically Nafion® or other perfluorinated polymers; electrodes are graphite felts (GFs) or carbon felts (CFs), and bipolar plates (BPs) are graphite plates. Although researchers are recently developing new materials, these materials are not yet used in commercial VRFB systems.

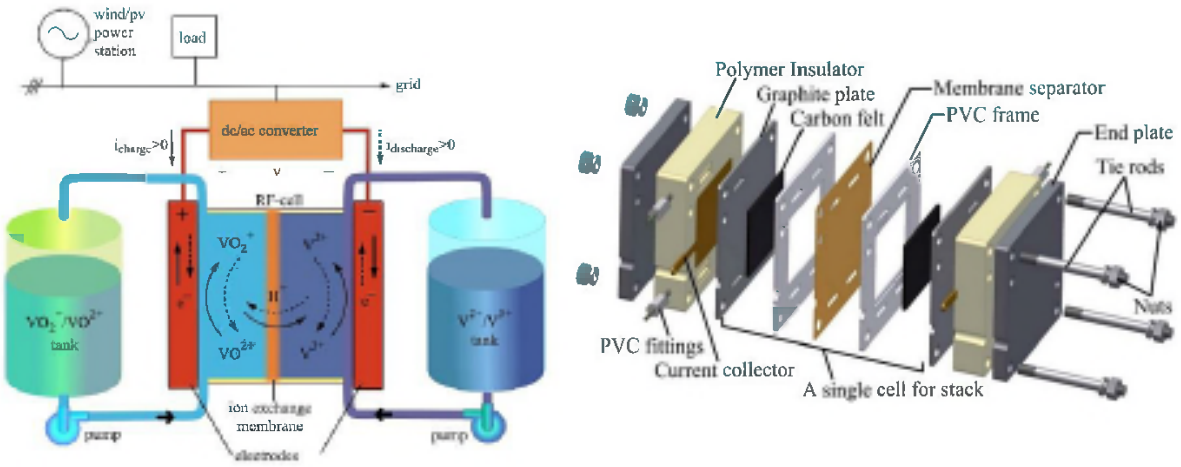

Figure 1 Diagrams of (a) a VRFB energy storage system with separated VRFB stack and electrolyte tanks [20] (Reproduced with permission from Elsevier); (b) a VRFB stack with its components [23] (Reproduced with permission from Elsevier)

In a VRFB, two simultaneous reactions occur on both sides of the membrane. The electrochemical reactions during charge and discharge are listed as follows:

Positive electrode reaction:

$$VO^{2+} + H_2O - e^- \overset{charge}{\underset{discharge}{\rightleftharpoons}} VO_2{}^+ + 2H^+ \qquad E_{cathode} = 1.004V \qquad (5)$$

Negative electrode reaction:

$$V^{3+} + e^- \overset{charge}{\underset{discharge}{\rightleftharpoons}} V^{2+} \qquad E_{anode} = -0.255V \qquad (6)$$

Overall electrochemical reaction of the cell:

$$VO^{2+} + H_2O + V^{3+} \overset{charge}{\underset{discharge}{\rightleftharpoons}} VO_2{}^+ + V^{2+} + 2H^+ \qquad E_{cell} = 1.259V \qquad (7)$$

During charging at the positive electrode, tetravalent vanadium within VO^{2+} ions (V(IV)) is oxidized to pentavalent vanadium within $VO_2{}^+$ ions (V(V)), while at the negative electrode trivalent ions V^{3+} (V(III)) are reduced to bivalent ions V^{2+} (V(II)). The hydrogen ions ($2H^+$) move through the membrane to maintain the electrical neutrality of the electrolytes. The standard open circuit voltage (OCV) of a VRFB cell is 1.26 V at 25 °C, but in reality, the cell exhibits an OCV of 1.4 V at 50% state of charge (SOC) due to proton activities, Donnan potential [24], and omission of other ionic species in the Nernst equation [25]. Considering the proton activities in the positive and anolyte and Donnan potential, the OCV can be calculated according to the following equation [24]:

$$V_{OC} = E_0 + \frac{RT}{nF}\ln\left[\frac{C_{V^{5+}}C_{V^{2+}}C^+_{H^+}(C^+_{H^+})^2}{C_{V^{4+}}C_{V^{3+}}C^-_{H^+}}\right] \qquad (8)$$

where R is the ideal gas constant (equal to 8.314 J mol^{-1} K^{-1}), F is the Faraday constant (equal to 95,484.56 C mol^{-1}), n is the number of moles of electrons transferred in the balance equation, T is the absolute temperature (typically 298 K), $C^+_{H^+}$ is the proton concentration at catholyte, and $C^-_{H^+}$ is proton concentration at anolyte. Typically, the VRFB is operated between 20 and 80% SOC, so the actual capacity is approximately 60% of the theoretical value. There are, in addition, several known side reactions, notably the evolution of oxygen in the positive electrode and the evolution of H_2 in the negative electrode on charge. Evolved H_2, in the form of bubbles, impacts performance through partial occlusion of the flow of the electrolyte, a reduction in the active surface area for reaction, and reduced mass and charge transport coefficients [26]. Evolved oxygen, in the form of bubbles, impacts performance by reducing the active surface area for electrochemical reaction in the electrode, reducing the effective diffusion coefficients, and lowering the effective ionic and thermal conductivities [27].

The VRFB was invented and developed by Maria Skyllas-Kazacos and her co-workers at the University of New South Wales. They successfully demonstrated the first commercial redox flow batteries employing vanadium in each half cell [28][29][30]. Since then, research on this technology has emerged all over the world and VRFB systems have become the most investigated RFB chemistry on a commercial scale [31].

Kear et al. [30] summarized the performance of VRFBs at the 1 kW to 1 MW scale; prototypes up to the range of MW in power and MWh in energy-storage capacity have also been demonstrated [1]. Currently, the largest scale VRFB system (200 MW/800 MWh) has been reported to being actively installed in China during 2017/8 [32].

VRFBs can be used for small scale applications (detached houses, for example); however, they are more suited to be employed for large-scale energy storage. Installations are often coupled with renewable energy sources, such as photovoltaic power plants or wind parks, or utilized for peak shaving or load shifting applications. These applications require not only a long term durability, but also a steady performance output.

1.3. VRFB degradation

VRFBs have been widely studied for storing intermittent renewable energies due to the following advantages [15][33]:

1) Vanadium is relatively abundant and the electrolyte solution is relatively easy to prepare;
2) The capacity can be easily adjusted by varying the solution volume and monitored by measuring the open-circuit cell voltage;
3) Unlike other secondary rechargeable systems, such as lead acid and lithium-ion batteries, VRFBs have very little environmental impact; the redox couple reactions do not generate any toxic gases and the batteries have a low risk of explosion;
4) Both the anolyte and the catholyte can be readily recycled;
5) The electrolyte acts as a secondary cooling system that allows heat to be readily extracted from the stack, which reduces the burden on thermal management systems;
6) Very fast recharging rates compared with conventional batteries;
7) The same reactive element and the same supporting electrolyte are used in both half-cells, limiting cross-contamination;
8) The VRFB system is considered very stable, offering long calendar life and unlimited electrolyte cycle life; the overall battery life is determined by the stability of the cell stack components.

To date, most studies have been devoted to the development of VRFB materials/components in an attempt to improve performance and reduce cost. A few excellent reviews have been published summarizing progresses of the VRFB development [21][22][30][34]. Reviews at a component level on electrolytes [33][35], electrodes [36], and membranes [37][38][39] can also be found.

The most important advantage of VRFBs is their durability and low-rate degradation. It is claimed that VRFBs have a cycle life over 12,000 cycles [40]. Although numerous demonstrations have further commercialized the VRFB technology, there are still some remaining challenges that need to be addressed or overcome. The high cost of vanadium electrolyte and membranes, the high purity requirements for the vanadium oxide raw material, and the electrode corrosion during overcharging all lead to decreased cell performance and increased stack material costs [33]. Overall, the key issue is the high cost of the VRFB system, roughly $500−600 per kWh [41]. To broadly penetrate the market, not only the capital cost but also the cycle life cost of VRFBs need to be substantially lowered [21]. While improving the performance of the VRFB cell/stack by exploring novel materials with lower cost could be the most effective way, further boosting of cell/stack durability shouldn't be underestimated to efficiently extend the operational life span; durability of the VRFB system is the major key to its future success. In fact, the degradation of the VRFB materials and the VRFB system has attracted much less attention to date than the performance improvement and a thorough literature search shows that only a few publications are available on the degradation of a VRFB or on stability tests of electrode material. Thus, the underlying basic science of the degradation for VRFB materials/components is not yet fully understood. Also, there have been no comprehensive reviews of the literature related to the VRFB degradation. As such, this paper reviews publications on performance degradation and mitigation strategies for VRFBs in an attempt to achieve a systematic understanding of VRFB durability with a focus on degradation of commercialized materials. It should be noted that this review is focused on component and cell-level durability issues, therefore issues of system integration are not examined, although they can be critically important for system commercialization.

The structure of this paper is as follows: after an introduction and short overview of RFBs and VRFBs, durability studies of individual VRFB components, including electrolyte, membrane, electrode, and BP, are presented. Various degradation mechanisms at both cell and component levels are examined. Following these, applicable mitigation strategies for alleviating degradation of each component are emphasized. In addition, this paper summarizes accelerated stress tests for VRFBs to prevent prolonged test periods and high costs associated with

real lifetime tests. To close, future research areas on the degradation and accelerated lifetime testing are proposed.

2. Degradation of VRFB components

Degradation of VRFBs can be caused by various reasons; for example, electrolyte contamination, electrode corrosion, corrosion of BPs, ion-exchange membrane breakage, and blockage of liquid pipe due to electrolyte crystallization [42][43]. To predict cell degradation is challenging as the VRFB system contains several key components with each component having its own degradation mechanisms. As such, mitigation strategies to reduce component degradation could be diversified. Although experimental data on the degradation mechanisms of the VRFB system are not extensively reported, this section aims to give a systematic overview of component degradation mechanisms, mitigation strategies, as well as diagnostic tools for performance and degradation.

2.1. Electrolyte

The electrolyte is one of the most important components of VRFBs. While the size of the stack decides the power of the VRFB, the electrolyte volume determines the battery capacity. In addition, the properties of the electrolyte could significantly affect the cell performance as well as the overall battery cost [33].

2.1.1. Commonly used electrolyte

The most commonly used redox couples in a VRFB system are V(II)/V(III) and V(IV)/V(V) (Equations (5) and (6)) in the negative and positive half-cell electrolytes, respectively. Skyllas-Kazacos and co-workers conducted a series of studies to screen various supporting electrolytes, such as HCl, H_2SO_4, and $HClO_4$. The results show that sulfuric acid offers the best combination of vanadium-ions solubility and redox-couple reversibility for VRFB applications [33]. Although the overcharge reaction in sulfuric acid would result in oxygen evolution, the produced gas is safe and environmentally acceptable. As such, H_2SO_4 has been chosen as the preferred supporting electrolyte for both the V(II)/V(III) and V(IV)/V(V) redox couples.

The capacity of a VRFB is dependent on the concentrations of the vanadium ions which, in turn, are dictated by the solubility of each of the redox couple ions V(II), V(III), V(IV) and V(V). The solubility of each ion is a function of temperature, sulfuric acid concentration, and SOC. The precipitation of V_2O_5 at elevated temperatures [44][45][46][47] and the low solubility of VSO_4, $V_2(SO_4)_3$, and $VOSO_4$ at low temperatures [48] limit the maximum vanadium ion concentration to 2 M, energy capacity to < 25 Wh kg^{-1}, and the operating temperature range to 10-40 °C [44]. This narrow operational temperature window, in particular its upper limit (40 °C), makes electrolyte temperature control necessary for practical applications.

In principle, vanadium electrolytes in a VRFB do not degrade and they shall remain the same even after the life of the VRFB energy storage system. The vanadium electrolytes recovered from an old VRFB at its end of life can theoretically be used for a new VRFB system. This is one of the advantages of the VRFB energy storage system, which makes the lifetime cost of the VRFB lower than competitive energy storage systems. In reality, the vanadium electrolyte does degrade during operation, affecting the efficiency and performance of the VRFB. The following sections address the loss of efficiency and performance caused by electrolyte degradation or changes related to the vanadium electrolyte.

2.1.2. Electrolyte degradation mechanisms

Electrolyte degradation is associated with vanadium chemistry, which is extremely complex. The complexity of the vanadium chemistry is attributed to the large number of different species existing at different potentials and pH values, as well as multifarious side reactions and processes. These reactions and processes include: (i) hydrogen evolution at the negative electrode; (ii) the oxidation of the V(II) ions in the presence of air at the

negative electrode; (iii) oxygen evolution at the positive electrode; (iv) vanadium ions transfer from one half-cell to the other; and (v) electrolyte transfer from one half-cell to the other due to pressure difference [35]. A better understanding of vanadium chemistry helps to comprehend electrolyte degradation. Major degradation mechanisms of the VRFB electrolyte include electrolyte precipitation, electrolyte impurities, and other changes related to the electrolyte.

2.1.2.1. Electrolyte precipitation

During the VRFB operation, all vanadium species (V(II) and V(III) in the anolyte and V(IV) and V(V) in the catholyte) may precipitate [45], causing potential blockages in the stacks and pumps and thus serious complications leading to component degradation that limits the energy density and capacity of the VRFB.

Electrolyte precipitation is closely related to the vanadium ion solubility and temperature stability. In other words, vanadium concentration in the VRFB electrolyte, a decisive factor for the energy density of VRFBs, is determined by the solubility and temperature stability of vanadium ions in different oxidation states and significantly influenced by the supporting electrolyte. To prevent precipitation of vanadium from potential blockages in the stacks and pumps, a maximum vanadium concentration should be employed over the operating temperature range. Skyllas-Kazacos and co-workers [33] summarized the solubility of each V(II), V(III), V(IV), and V(V) species in sulfuric acid at different temperatures and acid concentrations to help define these limits.

It has been identified that V(V) is the most unstable species among other vanadium species and most easily precipitates into crystals of V_2O_5 at a fully charged state of the VRFB cell. As a result, the V(V) chemistry and the V(V) stability have been the most studied topics for the VRFB electrolyte. Among various research groups, Maria Skyllas-Kazacos' group has been the most active in investigating how to increase the thermal stability of V(V) at different concentrations [44][49], precipitation phenomenon of V(V) at different temperatures, solution compositions and solution SOC [45], and precipitation inhibitors for supersaturated vanadyl electrolyte V(IV) [50]. They have also studied how to optimize the electrolyte in terms of concentration, temperature, precipitation behavior, density, and viscosity [47].

Vijayakumar et al. [51] have demonstrated that the V(V) species exists as a hydrated penta coordinated vanadate ion ($VO_2(H_2O)_3^+$). This molecule is stable at low temperatures but undergoes a deprotonation reaction at elevated temperatures forming the neutral $VO(OH)_3$ molecule which then undergoes a condensation reaction to form the V_2O_5 precipitate. This thermal precipitation reaction, reversible only by electrochemical means, is shown in Equations (9) and (10). Therefore, increasing the temperature decreases the stability of V(V) solutions as demonstrated by Rahman et al. [47] in Figure 2.

$$(VO_2(H_2O)_3)^+ \xrightarrow{\Delta} VO(OH)_3 + H_3O^+ \quad (9)$$

$$2VO(OH)_3 \rightarrow V_2O_5 \cdot 3H_3O \downarrow \quad (10)$$

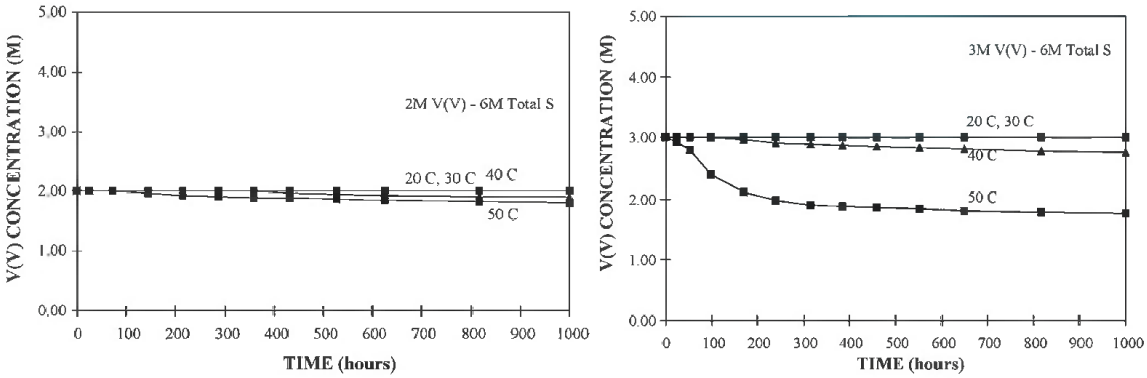

Figure 2 Stability of 2 M (left) and 3 M (right) V(V) solutions at different temperatures (Reproduced with permission from Elsevier)

In addition to the temperature, sulfuric acid concentration also plays a key role in stabilizing the V(V) solution. It has been observed that increasing total sulfate/bisulfate concentration results in an increased stability of V(V) solution. For example, at 40 °C, the apparent V(V) concentration of a 3 M V(V) solution is merely 1.6 M in 5 M sulfate/bisulfate whereas it is 2.8 M in 6 M sulfate/bisulfate [47]. The increased stability at higher sulfuric acid concentration is due to the higher H^+ ions favoring the backward direction of Equation (9).

Although higher sulfuric acid concentration is beneficial in promoting the stability of V(V), the limitation of sulfuric acid concentration arises from the lower solubility of V(II), V(III) and V(IV) at elevated sulfuric acid concentrations. The reduced solubility of these species is due to the common ion effect because, unlike V(V) which undergoes a thermal precipitation, each of these species precipitates as vanadium sulfate salts.

Zhao et al. [52] studied the solubility and the solubility parameters of V(III) species in the anolyte at various concentrations of H_2SO_4 and different temperatures. The results showed that dissolution of V(III) is an exothermic process and, as a result, the solubility of V(III) decreases with temperature (15-40 °C) and with prolonged exposure to lower temperatures. It was also found that a low concentration of H_2SO_4 can keep high concentration of V(III) stable for a long time. Specifically, the concentration of V(III) can reach 2.73 mol L^{-1} with 1 mol L^{-1} H_2SO_4 at 30 °C and be stable for at least 100 days [52].

Xiao et al. [53] studied the physical properties of V(II), V(III), V(3.5), V(IV), and V(V) at sub-zero temperatures. Results show that the low temperature precipitations can re-dissolve back into solution after being warmed to room temperature for 30 minutes, proving that the process is reversible. The same, however, does not apply to the V(V) precipitate where electrochemical means are required to re-dissolve the V_2O_5 precipitate back into solution. Such means may include reversing the cell polarity to convert V_2O_5 into V(IV) or V(III) or partially mixing the charged anolyte and catholyte to allow V(II) to electrochemically leach solid V(V) back into solution as V(IV) or V(II) [33].

The above results demonstrate that the solubility of V(II), V(III), and V(IV) decreases with decreasing temperature and increasing acid concentration while the opposite trends hold true for V(V). As a result, there has to be a balance in choosing the optimal temperature range, vanadium concentration, and sulfuric acid concentration for VRFB applications. Based on numerous studies by multiple research groups, the preferred electrolyte composition for the operating temperature range between 10 and 40 °C has been determined to be 1.6-2 M vanadium and 4-5 M total sulfate [33].

2.1.2.2. Effect of impurities

During the VRFB operation, impurities may be present in the vanadium electrolyte either from the raw material used to manufacture the electrolyte or from incompatible components within the system. Recently Cao et al. [54] published a thorough review on impurities and additives on VRFBs. The presence of impurities affects electrolyte stability, electrochemical kinetics, energy density, and overall cell performance.

Kubata et al. [55] measured the impact of Si and NH_4 on the VRFB performance. It was found that 40 ppm NH_4 in 2 M V / 2 M H_2SO_4 / 0.14 M H_3PO_4 / 4 ppm Si electrolyte distinctly slows the flow rate into the cell stack within 5 charge–discharge cycles, indicating NH_4 has deposited on the felt electrode and partially blocked the electrolyte flow. Lower concentrations of NH_4 (18 and 20 ppm) are found to have negligible effects. The same group observed a significant increase in cell resistance with the addition of 100 ppm Si to 2 M V / 2 M H_2SO_4 / 0.14 M H_3PO_4 / 18 ppm NH_4 electrolyte, high enough to make the system inoperable. A moderate but continuing increase in resistance was also observed with 50 ppm Si while 40 ppm causes no effect. The effect of Si on resistance is more profound within 1.7 M V / 2.6 M H_2SO_4 / 0.12 M H_3PO_4 / 20 ppm NH_4 electrolyte. While 40 ppm significantly increased the resistance, 10 ppm Si resulted in a step-change increase and 4 ppm showed no effect on the resistance. Although Kubata et al. were able to show the adverse impact of Si on VRFB cell performance, they did not provide any information regarding the mechanism of the degradation or whether the presence of NH_4 had an impact on the Si effects.

As part of his Master's Thesis, Burch [56] was able to supplement the work done by Kubata et al. Through scanning electron microscope/energy-dispersive X-ray spectroscopy (SEM/EDS) analysis, Burch confirmed that Si accumulated on VRFB electrodes and that the blockage was a physical phenomenon, not electrochemical; in this case, the electrodes acted as a filter, permanently removing particulates from the electrolyte. Burch, however, did not observe an increase in cell resistance at an estimated 14 ppm level of Si in 1 M V / 5 M H_2SO_4 and concluded that the additional NH_4 in Kubata's work had magnified the effects.

Burch also examined electrolytes prepared with $VOSO_4$ of increasing purity from various suppliers: American Elements ($3.52/g V), Alfa-Aesar ($4.10/g V), and Sigma-Aldrich ($27.86/g V); each included the analyzed impurities provided by the suppliers for comparison. Significant variation in performance was observed. Burch found that the least pure solution yielded the lowest performance while the most pure solution produced the highest performance. He also found that the blockage of electrode pores accounted for the performance variation of the three suppliers tested. In addition, the largest variation observed was in the mass transport area, demonstrating that impurities were impacting the reactant transport through the electrodes, reducing the operational window and capacity of the battery. To prevent the effect of impurities, he proved that filtration of low-purity electrolyte was able to remove the insoluble impurities, and thus improve current densities.

Some metals such as Ag, Cr, Cu, Fe, Mn, Mo, Ni, and Sn are known to catalyze the evolution of hydrogen which may impact the performance of VRFBs [33]. In particular, Ag, Cu, Ni, and Sn are certain to deposit on the negative electrode during charging as their standard reduction potentials are less negative than V(II)/V(III). Other impurities may also deposit within the pores of the membrane; however, as with other impurities, there is a lack of a systematic study in the public knowledge.

Recently Park et al. [57] performed a systematic study on the influence of impurities on VRFBs. Influence of alkali ions Li^+, Na^+, K^+, Mg^{2+}, and transition metal ions Fe^{2+}/Fe^{3+}, Co^{2+}, Ni^{2+}, Cu^{2+}, Zn^{2+}, and Mo^{6+} were investigated. It was found that most of the ions affect the V(II)/V(III) redox reaction rather than V(IV)/V(V), and that, among alkali ions, Li^+ decreases the VRFB performance the most, and Cr^{3+} and Ni^{2+} are the two transition metal ions significantly affecting the VRFB performance. Their effects are summarized in Table 1.

Table 1 Suggested specifications for metal impurities in the VRFB electrolyte [57] (Reproduced with permission from ECS)

Species	Concentration / M	Effect on vanadium reactions
Li^+	0.005	Retarding the kinetics of the V^{2+}/V^{3+} redox reaction
Na^+	-	Negligible effect
K^+	0.05	Decreasing the diffusion rate of V^{3+} ions
Mg^{2+}	-	Negligible effect
Cr^{3+}	0.005	Retarding the kinetics of the V^{2+}/V^{3+} redox reaction and decreasing the diffusion rate of V^{3+} ions
Mn^{2+}	0.02	Decreasing the diffusion rate of V^{3+} ions
Fe^{2+}/Fe^{3+}	0.05	Decreasing the diffusion rate of V^{3+} ions
Co^{2+}	0.05	Decreasing the diffusion rate of V^{3+} ions
Ni^{2+}	0.005	Retarding the kinetics of the V^{2+}/V^{3+} redox reaction and H_2 evolution
Cu^{2+}	0.001	Sedimentation in the negative electrolyte
Zn^{2+}	0.10	Decreasing the diffusion rate of V^{3+} ions
Mo^{6+}	0.001	Sedimentation in both the positive and negative electrolytes

2.1.2.3. Impacts caused by other changes related to the electrolyte

In addition to electrolyte precipitation and electrolyte impurity, the crossover of electrolyte is another form of electrolyte degradation in VRFBs. The crossover of electrolyte not only lowers the energy efficiency but also causes the imbalance of the vanadium species across the membrane. The amount of vanadium species that cross through the membrane depends on the type of membrane employed. As the crossover of electrolyte is closely related to membrane degradation, this will be discussed in details in membrane degradation.

During VRFB operation there may be other changes in the supporting electrolytes, for example, evaporation of solvent (water). These changes may also cause electrolyte degradation although the changes are expected to be very slow. So far, there are no studies reported on the impacts of these changes in the electrolyte.

2.1.3. Diagnostic tools for electrolyte degradation

2.1.3.1. Visual observation

A simple but crude method of diagnosing electrolyte degradation is via visual observation. This is possible due to the unique vanadium chemistry: distinct color changes of vanadium ions at different valent states. In aqueous solution, the solution color changes when vanadium ions undergo oxidations:

V(II) (violet) → V(III) (green) → V(IV) (blue) → V(V) (yellow)

Among vanadium ions at different valence states, V(V) is most stable whereas V(II) is least stable in the presence of air.

Within the same valence state, the color of vanadium solutions may also change. For example, the color of V(V) solutions in H_2SO_4 alters with the H_2SO_4 concentration: from green in 4 M H_2SO_4 to yellow in 4-5 M H_2SO_4, and further to yellow/red in 7-8 M H_2SO_4. This color change indicates that there exists a variety of V(V) complex species at different concentrations of V(V) and H_2SO_4, possibly due to changes in the coordination geometry of the V(V) complex [33].

Nevertheless, this unique feature not only allows visual observation of electrolyte degradation, but also estimation of the SOC of the solutions. To quantitatively analyze the electrolyte composition, a variety of techniques are available [33].

2.1.3.2. Electrolyte property measurement

In practical applications, the properties of the vanadium electrolyte will impact the characteristics, behavior, and performance of the vanadium battery, reflecting the degradation of the electrolyte. Important properties of the VRFB electrolyte include conductivity, density, and viscosity. These properties vary with supporting electrolyte composition, SOC, and temperature.

The conductivity of the electrolyte is an important parameter for all electrochemical cells as it contributes to the cell's ohmic resistance, which, in turn, affects the energy efficiency. The conductivities of the vanadium electrolytes have been measured as a function of vanadium and sulfuric acid concentrations [58][59]. In general, as the vanadium concentration increases for each of the vanadium ions, the electrolyte conductivity decreases due to the shift in the acid dissociation equilibria.

Another important property of the electrolyte is density. Mousa [60] measured the density of a series of V(III) sulfate solutions at different temperatures. The results show that a second-order model fits with respect to both the acid and V(III) sulfate concentration whereas a first order model fits with respect to temperature.

The viscosity of the VRFB electrolyte also plays an important role at both the cell and system level. Mousa [60] measured the viscosity of V(III) sulfate solutions (0.0-1.5 M V(III) sulfate and 1.0-2.0 M sulfuric acid) at temperatures between 15 and 40 °C. As expected, viscosity of the solution decreases with increasing temperature. This is explained by the increase in the kinetic energy of the species in solution and less solute–solvent and solute–solute interactions, leading to a decrease in resistance/friction against the flow of the solution at a high temperature.

2.1.3.3. Quantitative/qualitative analysis of vanadium ions solutions

As aforementioned, the chemistry of vanadium electrolytes is quite complex, especially in the V(IV) and V(V) oxidation states. Considerable research has been carried out to understand vanadium chemistries in solutions of vanadium/sulfuric acid. As such, quantitative measurements of vanadium ions at different oxidation states and their concentrations are important in understanding vanadium chemistries in operating VRFBs. Spectroscopic tools such as Ultraviolet (UV) spectroscopy, Raman spectroscopy, and nuclear magnetic resonance (NMR) have been evaluated for quantitative and qualitative analyses of VRFB electrolytes.

Due to the distinctive color differences, UV visible (UV/Vis) spectroscopy can be used for analyzing each of the vanadium ions in sulfuric acid [61]. Brooker et al. [62] described the method in detail to generate quantitative concentrations of different vanadium ions in a VRFB. In terms of the ion concentration values, the UV/Vis method has proven to be more reliable than either the electrode voltage or the integrated current with respect to time. Typical UV spectra for the vanadium electrolytes can be found in Choi et al.'s review paper [35]. For the V(IV) electrolyte, absorbance at 750 nm [63] or 765 nm [64] was selected for a quantitative analysis. For V(II), V(III), and V(V) ions, absorbance at 855 nm, 610 nm, and 390 nm was used, respectively. UV can also be used for monitoring the SOC. For the anolyte, a linear relationship between the absorbance at 750 nm and the SOC was found over the SOC range of 5-100% [63].

NMR spectroscopy is a powerful tool to study the vanadium chemistry in sulfuric acid solutions. ^{1}H, ^{17}O, and ^{51}V NMR spectroscopy have been used to study the coordination structure and dynamics of the molecules in VRFB electrolytes. Owing to its diamagnetism, the only oxidation state of vanadium ions active in ^{51}V NMR is V(V). The other oxidation states (V(II), V(III), and V(IV)) are paramagnetic, resulting in an extreme broadening of the vanadium NMR lines. Vijayakumar and co-workers [51] applied ^{17}O and ^{51}V NMR spectroscopy and density functional theory (DFT)-based computational modeling to investigate the solubility of V(V) electrolyte solution. The same research group also conducted ^{1}H and ^{17}O NMR analyses for a V(IV) electrolyte with varying vanadium concentrations and temperatures [65]. Electrolytes were analyzed depending on the chemical shift and line width.

These two parameters are directly associated with the electronic atmosphere and mobility of atoms. As the electron density in the molecular orbitals decreased, the chemical shift increased due to a reduced shielding effect while the line width of the NMR peak increased with decreasing molecular mobility [35].

Raman spectroscopy is also a useful tool to monitor changes in the V–O bond. Characteristic peaks include V–O terminal stretching (800-1000 cm^{-1}), V–O bridging mode (400-800 cm^{-1}), and V–O bending and lattice modes (below 400 cm^{-1}). Several studies on the chemistry of vanadium compounds were carried out by using Raman spectroscopy. Griffith and co-workers [66][67][68] conducted a thorough investigation of the chemical composition of 2.0 M V(V) solutions over the entire pH range (1-14). Madic and co-workers [69] investigated the chemical composition of V(V) solutions in highly concentrated sulfuric acid and perchloric acid solutions. Kausar and co-workers [49] studied the chemistry of supersaturated solutions of V(V) and V(IV) in highly concentrated sulfuric acid solutions. The Raman spectra of mixed solutions of V(IV) and V(V) ions was also investigated by Kausar et al. For V(V) electrolytes, the broad peaks from V–O–S bridging stretching at 660-680 cm^{-1} and V–O–V stretching (770 cm^{-1}) increased with vanadium concentration, in good agreement with the high temperature instability at high vanadium concentrations for the V(V) electrolyte [49].

Other methods that can also be used for the quantitative analysis of total vanadium concentrations include atomic absorption spectroscopy and inductively coupled plasma analysis [33].

2.1.4. Mitigation strategies for electrolyte degradation

2.1.4.1. Precipitation inhibitors

Based on the electrolyte degradation mechanisms, one of the most important mitigation strategies would be to prevent the precipitation of the vanadium ions by controlling the electrolyte concentration. For example, the solubility of the V(II), V(III), V(IV), and V(V) ions limit the practical concentration of the VRFB electrolyte to 1.6-1.8 M for an operating temperature range of 10-40 °C. To prevent thermal precipitation, a total sulfate concentration closer to 5 M is recommended to stabilize V(V) for warm climates. A lower total sulfate concentration closer to 4 M is preferred to minimize the risk of precipitation of V(II) and V(III) ions for cold climates.

For supersaturated high concentration solutions, precipitation inhibitors could be used as an important mitigation strategy in order to stabilize vanadium ions and prevent their precipitations during charge–discharge cycling of the VRFBs. Skyllas-Kazacos and co-workers proved that precipitation inhibitors could be successful [48][70]. Numerous research groups have studied a wide range of organic and inorganic additives as precipitation inhibitors for supersaturated V(II), V(III), V(IV), and V(V) electrolytes, although most organic additives were unstable in the presence of highly oxidizing V(V) species [33]. For example, ammonium phosphate, ammonium sulfate, Flucon100, sodium pentapolyphosphate, and glycerol additives have been investigated. Cell cycling experiments confirmed that ammonium phosphate could dramatically extend cell operation of a 2 M solution of vanadium without precipitation over more than 250 cycles at 5 °C, compared with less than 15 cycles for a solution without additives [71]. The use of H_3PO_4 to reduce V(V) precipitation at higher temperatures was also well recognized. Roe et al. [72] found adding 1 wt% H_3PO_4 to a 3 M V(V) / 5 M H_2SO_4 solution increased the induction time of V_2O_5 precipitation from 3 days (blank) to 47 days; higher concentrations (2-3%) were found to have little beneficial impact. Kausar et al. [73] observed that with the addition of 1% phosphoric acid to the VRFB electrolyte, induction times of 40, 22, and 18 days were achieved for 80, 90, and 95% SOC solutions at 50 °C, compared with 5, 2 and 1 days, respectively, for the corresponding blank solution. Skyllas-Kazacos and co-workers [50] also found that additives, such as K_2SO_4, $(NaPO_3)_6$ and CH_4N_2O (urea), could be effectively used as precipitation inhibitors when the concentration was below a certain level, at which reactions with the V(IV) ion may occur.

2.1.4.2. Alternative electrolytes

To ensure long electrolyte life, alternative aqueous and nonaqueous solvents and supporting electrolytes may create a new pathway to high energy density chemistries, although sulfuric acid is often used in the VRFB technology to obtain a highly concentrated V(V) solution. Great efforts have been made to develop alternative electrolytes, such as non-aqueous or weak acidic electrolytes, which meet the requirement for a long electrolyte life [74]. Note that, to ensure long electrolyte life, any new chemistry requires the same active material in both half-cells in order to prevent diffusion across the membrane and, therefore, any additives or complexing agents for enhancing solubility must be compatible with both half-cell reactions [33].

Lee et al. [74] developed a novel cathodic V(IV)/V(V) electrolyte based on oxalic acid ($H_2C_2O_4$). This $H_2C_2O_4$-based electrolyte significantly improved redox reversibility and reaction kinetics with impressive charge–discharge capacities. The high charge–discharge capacities were believed to result from the redox reaction of both $V(Ox)_2$/ V(Ox) (vanadium chelate) and $[VO(H_2O)_5]^{2+}$/$[VO_2(H_2O)_4]^{+}$ couples in the cathodic oxalic acid electrolyte. The use of this novel cathodic electrolyte provides a potentially useful approach to prevent electrolyte degradation and enhance cell performance. Nevertheless, further studies are still required in terms of long-term stability, the reaction mechanism, and the possibility of organic decomposition for the electrolyte based on $H_2C_2O_4$.

Vijayakumar et al. [75] investigated the V(V) cation structures in mixed acid (hydrochloric and sulfuric) based electrolyte. The solution was analyzed by computational modeling based on the DFT and ^{51}V and ^{35}Cl NMR spectroscopy. The results showed that the V(V) cation exists as a di-nuclear $[V_2O_3Cl_2{\cdot}6H_2O]^{2+}$ compound at higher vanadium concentrations (≤1.75 M). It was found that the increase in temperature facilitated the formation of the chlorine bonded di-nuclear compound via ligand exchange process. Due to the formation of chlorine bonded vanadium species, the thermal stability of V(V) cations in mixed acid system is enhanced, which in turn prevents the de-protonation and subsequent precipitation reactions.

2.1.4.3. Electrolyte additives

For a stable VRFB, substantial research has been conducted in terms of electrolyte additives.

Influence of several additives on the stability of V(V) electrolyte for VRFBs was studied by Wang et al. [76]. Stability of the V(V) electrolyte with and without additives was investigated over a wide temperature range of -5 to 60 °C. The results showed that methyl orange, Triton X-100, sodium ligninsulfonate, sodium dodecyl sulfate, and polyvinyl alcohol significantly all independently improved the stability of the V(V) electrolyte across a wide range of temperatures. In addition, all of these additives also displayed improved electrochemical activity when compared to the pristine solution.

Ding et al. [77] investigated a series of phosphates as additives to improve the stability of the VRFB electrolyte. It was demonstrated that $NH_4H_2PO_4$ additives significantly improved redox reaction reversibility and activity, as well as energy efficiency. Further, the cell with $NH_4H_2PO_4$ additives in the electrolyte exhibited a much slower charge capacity fading rate in comparison to the cell without additives during cycling at high temperature. The results indicate that the long-term stability and durability of VRFBs are improved by the phosphate additives, reducing the electrolyte maintenance cost for long-term operation.

2.1.4.4. Electrochemical means

Sometimes, the precipitation of vanadium ions is inevitable due to unexpected temperature drift, supersaturation, or the formation of intermediate species. Once precipitation occurs, the V(II), V(III), and V(IV) salts may be redissolved by increasing the temperature. However, this strategy does not apply to any V(V) precipitate that might form at elevated temperatures. In this case, electrochemical means may be employed to redissolve any V(V) precipitate: for example, i) electrochemically convert any solid V(V) into more soluble V(IV) or V(III) ions by

reversing the cell polarity, or ii) electrochemically leach solid V_2O_5 back into solution as more soluble V(IV) or V(II) species by partially mixing the charged positive and negative solutions [33].

2.2. Membrane

2.2.1. Functions and properties of membranes

The VRFB membrane is a semipermeable membrane generally made from ionomers or polymers. It is designed to be a separator between the anode and cathode compartments to separate the active species. In the meantime, it also acts as an electronic insulator and an ionic conductor, facilitating the transport of ions such as protons or sulfate ions to maintain charge balance within the cell. The demands for the membrane are stringent: high ion exchange capacity or high ionic conductivity, low vanadium ion permeability, low cost, optimal water transfer properties, and long-term chemical stability under VRFB operating conditions. A high proton conductivity and low vanadium ion crossover could improve VRFB's coulombic efficiency (CE), leading to high overall efficiency. Optimal water transfer properties could avoid precipitation of vanadium salts in the cell and flooding of the solution reservoir. Long term chemical stability of the membranes in charged electrolyte solutions is of great importance for the durability of VRFBs.

In general, membranes can be classified based on factors such as the nature of the material, morphology, and pore size. According to the type of ionic functional groups attached to the membrane backbone, ion exchange membranes can be categorized into cation exchange membranes (CEMs), anion exchange membranes (AEMs) and amphoteric ion exchange membranes [78]. Cation exchange membranes contain negatively charged groups, such as $–SO_3^-$, $–COO^-$, $–PO_3^{2-}$, $–PO_3H^-$ and $–C_6H_4O^-$. They provide passages for cations, such as Na^+, whereas they are non-permeable to anions like Cl^-. Anion exchange membranes have positive functional groups, such as $–NH_3^+$, $–NRH_2^+$, $–NR_2H^+$, $–NR_3^+$, and $–SR_2^+$, and thus allow the passage of anions. Amphoteric ion exchange membranes, also called bipolar membranes or composite membranes, can be produced to contain a cation selective layer (with negative fixed ionic groups) and an anionic selective layer (with positive ionic groups).

Various membranes have been investigated for VRFB applications. Currently, the most widely used are Nafion® membranes; however, they have several disadvantages, such as high cost (US \$200-500/m^2) and high vanadium crossover. In order to reduce the cost and extend the lifetime of VRFB membranes, great efforts have been made by researchers in the VRFB research and development community. In addition to modifying Nafion® membranes [79][80][81][82], alternative membranes have also been developed, including other polymeric CEMs, such as polyether ether ketone (PEEK) [78] and sulfonated diels-alder poly(phenylene) [83], AEMs [84][85], amphoteric ion exchange membranes [86][87][88], and microporous separators such as Daramic membranes and Amer-Sil membranes [89][90][91][92]. Even if modifying Nafion® membranes could enhance the chemical stability, it would not reduce the overall cost of the membrane iteslf; thus, research efforts are being focused on alternative perfluorinated acid membranes, new anion-exchange membranes, and other types of polymer membranes. However, at the current stage, only perfluorinated membranes are commercially used in VRFB cells or stacks.

2.2.2. Membrane degradation mechanisms

The VRFB is known to degrade in performance over time. Membrane degradation in extreme chemical environments is one of the major factors leading to reduced capacity or increased internal resistance. The crossover rate of vanadium ions through the membrane, water transport property, and chemical stability of the membrane strongly affect the membrane durability in VRFBs.

2.2.2.1. Vanadium ions crossover

Vanadium ion crossover represents the diffusion of vanadium ions across the membrane, which will lead to self-discharge and side reactions at the positive and negative electrodes, affecting the VRFB capacity over long term

charge–discharge cycling. Depending on the SOC, the catholyte contains a mixture of V(IV) and V(V) ions while the anolyte contains V(III) and V(II) ions. This results in concentration gradients of each ion across the membrane, motivating the diffusion of each species from one half-cell to the other during cycling. The rate of crossover of the vanadium ions provides an insight on how to optimize operating conditions to reduce the crossover of vanadium ions and thus enhance the durability of VRFBs.

Agar et al. [93] used a 2-D transient model to study the ion transport mechanisms responsible for vanadium crossover of VRFBs. It was found that the instantaneous transport of vanadium across the membrane during charging and discharging caused side reactions which decreased the system's CE. The magnitude of the vanadium ion diffusion determines the rate of the self-discharge reactions. Even if the vanadium transport during charging is exactly equal to the vanadium transport during discharging in the opposite direction, the cell will not maintain 100% CE. The side reactions associated with species crossover is listed in Table 2 [93].

Table 2 Side reactions incorporated at the membrane/electrolyte interface [93] (Reproduced with permission from Elsevier)

Cross over Species	Reaction location	Side reaction
VO^{2+}	Negative half-cell	$VO^{2+} + V^{2+} + 2H^{+} \rightarrow 2V^{3+} + H_2O$
VO_2^{+}	Negative half-cell	$VO_2^{+} + 2V^{2+} + 4H^{+} \rightarrow 3V^{3+} + 2H_2O$
V^{2+}	Positive half-cell	$2VO_2^{+} + V^{2+} + 2H^{+} \rightarrow 3VO^{2+} + H_2O$
V^{3+}	Positive half-cell	$VO_2^{+} + V^{3+} \rightarrow 2VO^{2+}$

Zhang's group [94][95] found that the vanadium crossover was closely related to the self-discharge of VRFBs. They also found that the crossover of vanadium ions was mainly due to the concentration difference of vanadium ions between the catholyte and anolyte, leading to a decreased OCV value as long as the electrolyte flows continually through the two surfaces of the membrane.

Vanadium ion crossover is also accompanied by other ions to maintain electric neutrality, leading to capacity decay. Sun et al. [96] investigated the transfer behavior of different ions across the VX-20 AEM and the Nafion® 115 CEM under VRFB operating conditions. It was found that V(II) ions accumulated at the negative side when the cell was assembled with Nafion® 115, while the V(IV) ions accumulated at the positive side for VX-20. To balance the charges, the SO_4^{2-} ions transferred across Nafion® 115 while the protons transferred across VX-20 membrane. The capacity decay of the VRFB assembled with Nafion® 115 mainly resulted from the cross mixing of vanadium ions across the membrane; however, for VX-20, the side reactions were the major reason. Figure 3 shows the diagrams of the ion transfer between the positive and negative sides of the membrane [96]. Note that the diagrams give an overall direction only. During operation, the transfer direction could be different during the charge and discharge processes.

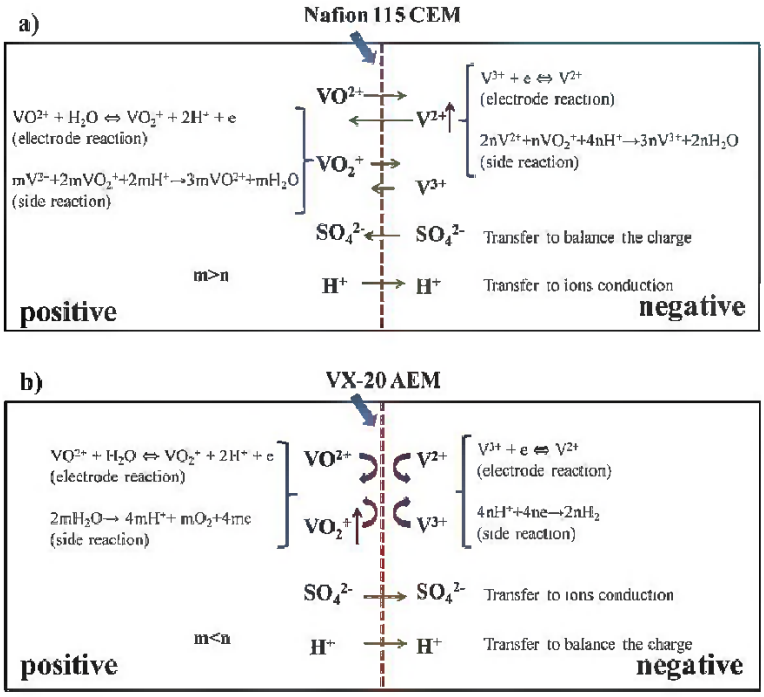

Figure 3 Diagrams showing different ions across a) Nafion® 115 and b) VX-20 membrane during the charge–discharge process [96] (Reproduced with permission from Elsevier)

Convection, resulting from electrolyte hydraulic pressure differentials at both sides of the membrane, is also considered to have a dominant effect on vanadium crossover and capacity decay while cycling. Li et al. [97] studied the capacity decay mechanism of VRFBs using microporous separators as membranes. They determined that the capacity decay was due to an asymmetrical valance of vanadium ions caused by the subsequent disproportionate self-discharge reactions at both sides of the separator. Although the concentration of total vanadium ions remained nearly constant at both sides over cycling, there was a net transfer of solution from one side to the other. Nevertheless, the rate of vanadium permeation through the membrane was very small in comparison to the transport rates associated with migration under current.

Recently, some mathematical modeling work has been done to simulate the accumulation of vanadium ions and predict the capacity loss over the course of many cycles. For example, Skyllas-Kazacos et al. [98] modeled the concentration profiles of different vanadium ions across a CEM as a function of time under different charge and discharge currents. A build-up of the total vanadium ion concentration in the positive half-cell was predicted, in agreement with observed trends in laboratory prototype VRFB systems. This proves that unequal rates of diffusion across the ion exchange membrane gives rise to capacity loss due to a build-up of vanadium ions in one half-cell with a corresponding decrease in the other. Through 45 cycles, simulation of both Nafion® and s-Radel CEMs, Agar et al. [93] also observed a net transfer of vanadium from the negative to positive half-cell, which was responsible for the loss in capacity. They concluded that the operating conditions, together with diffusion, convection, and migration could significantly influence the rate and direction of crossover during the VRFB operation. The modeling work of Elgammal et al. [99] propounded that, under current, the transport rates associated with migration was much higher than the rate of vanadium permeation through the membrane.

In general, the state of vanadium electrolyte and the transfer behavior of different ions are closely related to the ion exchange membranes. The characteristics of membranes, e.g. the functional charged groups, the backbone, the micro structures, greatly affect their transfer behaviors.

2.2.2.2. Water transfer

Water transfer is another important source of performance degradation over cycling either due to precipitation of vanadium salts in the cell or flooding of the solution reservoir [100]. There is a net volumetric water transfer across the membranes during charge–discharge cycling of the VRFB and studies have shown that the direction of the volumetric transfer is dependent upon the nature of the ion exchange membrane used [100][101]. For a cell employing an AEM it was observed that the net volumetric water transfer is toward the negative half-cell, whereas for CEMs the net volumetric water transfer is toward the positive half-cell.

The direction of water transfer is also dependent on the SOC of the vanadium electrolytes employed [102]. Sukkar et al. [102] reported that when the vanadium electrolytes were at between 100 and 50% SOC, the direction of water transfer was towards the positive half-cell. As the electrolyte self-discharged from 50 to 0% SOC, the direction of water transfer reversed toward the negative half-cell. The most significant level of water transfer occurred when the cell went into over-discharge where the V(III) and V(IV) electrolytes became fully mixed below the 0% SOC state.

Water transfer across the membranes can be caused by a number of processes, including water transported by ions moving under a concentration gradient, water carried by the charge balancing species, and water transport due to the osmotic pressure difference between the two half-cell solutions. The contribution from each process varies for different membranes and vanadium electrolytes, giving a different level of net water transfer for each membrane [101].

2.2.2.3. Membrane chemical stability

The membrane's chemical stability plays an important role in VRFBs' long service due to the harsh chemical environments (high concentration of supporting H_2SO_4 electrolyte and high oxidative reactive species) [37][103][104][105].

Mohammadi et al. [106] studied the chemical stability of Daramic, modified Daramic, and commercial ion exchange membranes during charge–discharge cycling by monitoring the membrane resistivity and permeability to identify any changes due to membrane fouling or degradation. It was found that chemical degradation is associated with the oxidation of the polymeric membrane material by the catholyte. Huang et al. [104] studied sulfonated polyimide (SPI) membrane degradation in VRFBs. They found that after 800 cycles, the SPI membrane was visibly fractured, resulting in the VRFB failure. Optical and SEM examinations of the membrane showed that the membrane surface facing the positive electrode contained considerable microdefects, while the surface facing the negative electrode did not change, as shown in Figure 4. The strongly oxidative V(V) species and strong acidic environment were considered to be responsible for the membrane degradation; evidence of this comes from the generation of V(IV) (the reduction product of V(V)) observed alongside degradation [102]). Kim et al. [103] investigated the chemical degradation of a sulfonated poly(sulfone) membrane during charge–discharge cycling in the VRFB cell. They found that the membrane suffered from delamination on the surface in contact with the positive electrode. A vanadium-rich region and a loss in the sulfonate SO_2 stretch intensity were both observed near the degraded surface.

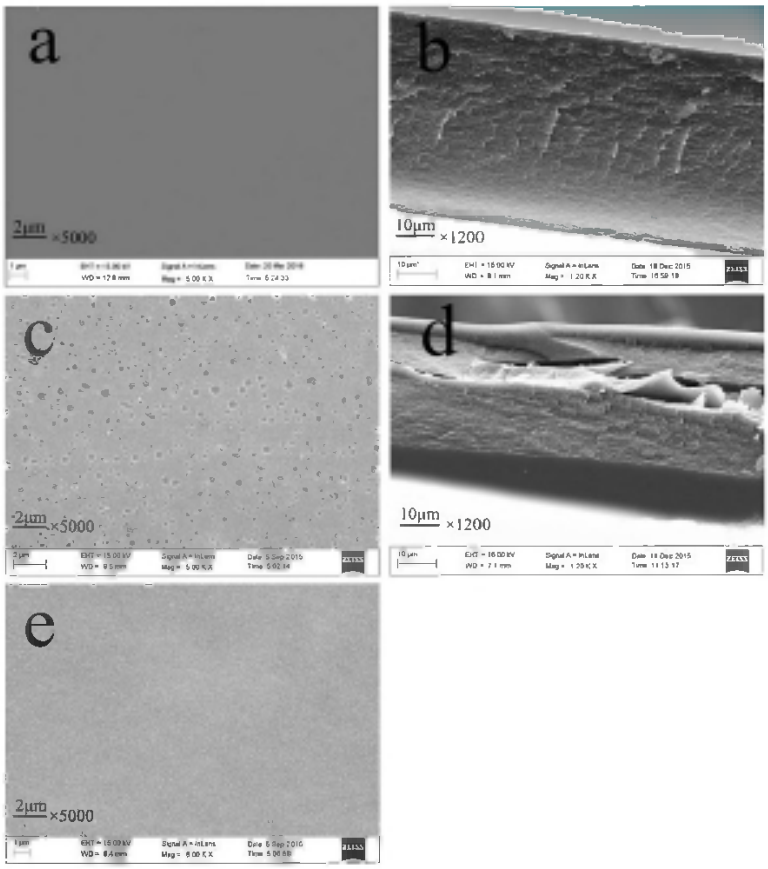

Figure 4 SEM image of SPI-H membrane: (a and b) initial surface and cross-section respectively before VRFB test; (c) surface facing the positive electrode after VRFB test; (d) cross-section after VRFB test; (e) surface facing the negative electrode after VRFB test [104] (Reproduced with permission from Elsevier)

2.2.3. Diagnostic tools for membrane degradation

2.2.3.1. Vanadium ions crossover measurement

The crossover of vanadium ions cannot be avoided if electrolytes flow continuously at both sides of the membrane. The vanadium ions that do cross over could cause undesired contamination and energy losses in the VRFB system. To predict the VRFB degradation, it is crucial to measure and quantify these crossover rates.

Heintz et al. [107][108] built a dialysis cell consisting of two half cells separated by the membrane to measure the diffusion coefficients of vanadium ions; atomic absorption spectrometry and ion chromatography were used as analytical tools. The experimental data of exchange diffusion and exchange equilibria were then used to study the diffusion velocity of the mobile ions in the membrane on the basis of the Maxwell-Stefan formalism of multicomponent diffusion processes.

A standard test procedure to measure vanadium ion crossover was developed by Skyllas-Kazacos and co-workers [78][102]. To eliminate any interference from water transport due to osmotic pressure effects across the membrane, *ex-situ* testing procedures were also developed [78][94][95][102]. Typically, the membrane is sandwiched between two half-cells with gaskets on either side to prevent solution leakage [99]. One half-cell contains $VOSO_4$ solution, and the other half cell contains $MgSO_4$ solution. The $MgSO_4$ solution (initially free from $VOSO_4$ ions) is sampled periodically to measure the V(IV) concentration using a UV/Vis spectrophotometer,

which gives the permeability of the V(IV) ions through the membrane. The rate of V(IV) ion diffusion is determined by the rate of change in the absorbance according to the following equation [78].

$$\ln[absB_0 - 2absA] = \ln[absB_0] - \frac{2k_sAt}{V_A} \quad (11)$$

where $absB_0$ is the initial absorbance of solution B, absA is the absorbance of solution A, A is the area of the membrane exposed, t is time, and V_A is the volume of solution A. The slope of a plot of $\ln[absB_0 - 2absA]$ versus t determines the mass transfer coefficient (k_s) of the V(IV) ions across the membranes. The plot should be linear and has a slope equal to $-2k_sA/V_A$. The diffusion coefficient, D, is thus calculated using the following equation:

$$D = k_s dy \quad (12)$$

where y is the thickness of the membrane. Diffusion coefficients of vanadium ions through different membranes are shown in Table 3 [109].

Table 3 Diffusivity of four vanadium species in several membranes [109]

Membrane	Diffusivity / cm min^{-1}			
	V(II)	V(III)	V(IV)	V(V)
AMV	2.01×10^{-6}	1.11×10^{-6}	3.17×10^{-5}	5.67×10^{-5}
CMV	1.01×10^{-5}	1.34×10^{-5}	2.65×10^{-5}	2.14×10^{-4}
Nafion® 117	4.63×10^{-5}	4.24×10^{-5}	1.94×10^{-4}	1.41×10^{-4}
Daramic (0.15 mm)	6.21×10^{-4}	7.09×10^{-4}	1.46×10^{-3}	$> 1 \times 10^{-2}$
Composite membrane (0.23 mm)	1.26×10^{-4}	1.34×10^{-4}	3.64×10^{-4}	2.92×10^{-3}

Using this method, Sun et al. [96] measured the vanadium crossover rate during VRFB operation. The positive and negative electrolytes were sampled at the end of discharge at various cycles and subsequently tested via auto potentiometric titration to determine the change in vanadium ions. Elgammal et al. [99] monitored concentration changes of vanadium ions for permeability measurements. In addition to vanadium crossover measurement, Agar et al. [93] created a 2-D transient VRFB model to distinguish the relative contribution of diffusion, migration, osmotic and electro-osmotic convection to the net vanadium crossover. The simulation results suggest that convection is an important mechanism of species transport which affects the direction and magnitude of crossover.

2.2.3.2. Water transfer measurement

A standard water transfer test cell was developed [78][101] to monitor the net water transfer across the membrane. Clear Perspex was used to construct the cell, which contained two half-cells with a cavity. The test membrane was pressed between the two half-cells. The ports adjacent to the Perspex tubes were used to transfer solutions to the cavities. Initially, the solutions were at the same level, and the deviations were recorded periodically.

Sun et al. [95] measured water transfer across the Nafion® 115 membrane in an operating VRFB stack (15 cells, 875 cm^2 each). They studied water transfer in both the self-discharge process and charge–discharge cycles. For the former, after charging to 23.25 V, the stack was started to self-discharge. The volume of catholyte and anolyte were recorded every few hours to measure the water transfer across the membrane. In the cycling experiments, the stack was charged to an upper limit voltage of 23.25 V and was discharged to a lower limit voltage of 15 V for each cycle. The volume of catholyte and anolyte were recorded every 10 cycles.

2.2.3.3. Chemical stability test

For membrane stability evaluations, immersion of membranes in V(V)-containing electrolyte is the most efficient and effective method, especially at elevated temperatures, which accelerate the chemical degradation of the membrane and shorten the experimental duration [102][110][111]. Typically, a pre-weighed membrane with a known area is soaked in a known volume of V(V) solution. Membrane oxidation by V(V) ions produces blue V(IV) ion species, which is used as an indicator for membrane stability measurement. V(IV) concentration can also be determined by UV/Vis spectrophotometry. By periodically monitoring V(IV) concentration, the membrane oxidation rate can then be obtained.

When Sukkar and Skyllas-Kazacos [102] studied the membrane stability, they found that the resistivity of membranes decreased after being soaked in a 0.1 M V(V) + 0.25 M H_2SO_4 solution for extended periods of time, possibly due to erosion of the polymeric material. The ion exchange capacity (IEC) of membranes was found to increase with soaking time; this might be explained by the anions (SO_4^{2-} and HSO_4^-) from the solution lodging in the pores of the membrane. The V(IV) ion diffusivity of membranes was adversely affected by extended exposure to the solution. The results from the long-term stability tests indicated that the faster rate of ion transfer should likely take the credit for the decrease in resistance of the membrane and, although the weight loss and degree of oxidation was low, all of the membrane properties gradually deteriorated over time. Huang et al. [104] found that both H^+ and V(V) played important roles in accelerating the membrane decomposition. Higher H^+ and higher V(V) concentrations resulted in faster SPI membrane degradation.

2.2.4. Mitigation strategies of membrane degradation

In terms of membrane degradation, several strategies have been applied to mitigate vanadium crossover, water transport, and loss of chemical stability [78].

2.2.4.1. Modification of Nafion®

The instantaneous transport of vanadium across the membrane during charge and discharge can be mitigated by minimizing imbalances of species concentration between half-cells during cycling, thereby extending the lifetime of a VRFB. This requires further control of the specific transport properties of the membrane. As such, hybrid and composite membranes have been functionalized to extenuate vanadium crossover [79].

Cha et al. [79] reviewed recent developments of nanostructured membranes for VRFBs. Modifications of Nafion® seem to be effective in decreasing vanadium crossover; for example, coating Nafion® with charged substances (Polycations and Polyanions) was found to be able to reduce the permeation of vanadium ions [80]. Comparing modified membranes with the unmodified Nafion®, it was observed that after modification, the crossover of vanadium ions through the membrane was dramatically reduced and the resistance of the membrane slightly increased. Another approach involves the fabrication of a barrier layer onto the surface of Nafion® by alternate adsorption of polycation, poly(diallyldimethylammonium chloride), polyanion, and poly(sodium styrene sulfonate) using a polyelectrolyte layer-by-layer self-assembly technique. This barrier layer helped suppress the crossover of vanadium ions [81]. Skyllas-Kazacos et al. [78] reported that the Nafion®/inorganic oxide nanoparticle hybrid membrane could dramatically reduce vanadium ion permeability and exhibit a lower self-discharge rate with high coulombic, voltage, and energy efficiencies. Polymer blending is also an effective method for polymer modification. Earlier, Nafion®/polyvinylidene fluoride (PVDF) blends were utilized to prepare CEMs for VRFB systems. The addition of the highly crystalline and hydrophobic PVDF seemed to effectively control the swelling of Nafion®, reducing the crossover [82].

Considering membrane degradation, chemical stability is a major concern for the extended lifetime of a VRFB. Commercially, Nafion® and modified Nafion® seriesbased ion exchange membranes have been used for VRFBs by Prudent Energy, Rongke Power, and UniEnergy Technologies (UET) [15]. To achieve a lower vanadium crossover and better chemical stability, the fluorinated CEM has been reported. Wei et al. [112] have

demonstrated that PVDF ultrafiltration membranes offer good performance and excellent stability in VRFB applications. No performance decrease was observed for PVDF membranes after more than 1000 cycles in a charge–discharge test. Poly(vinylidene fluoride)-graft-poly(styrene sulfonic acid) (PVDF-g-PSSA) CEMs were prepared by Luo et al. [113] using a solution-grafting method. Due to the high conductivity and dramatically low vanadium ion permeability, the VRFB with the low-cost PVDF-g-PSSA membrane exhibited a higher performance compared to Nafion® 117 under the same operating conditions with energy efficiency reaching 75.8% at 30 mA cm^{-2}. The performance of a VRFB with the PVDF-g-PSSA membrane was found to be stable even after 200 cycles at a current density of 60 mA cm^{-2}. Another partially fluorinated CEM was prepared by Qiu et al. [114] via radiation grafting of styrene and maleic anhydride onto the PVDF membrane followed by sulfonation. The grafted membrane exhibited a much lower permeability than Nafion® 117. Moreover, the OCV was maintained above 1.3 V after 33 h, much longer than that with Nafion®.

2.2.4.2. Alternative membranes

More recently, hydrocarbon-based AEMs have been considered for VRFB applications since they offer solutions to many of the problems found with Nafion®. For example, Sandia National Laboratories reported the development of poly(phenylene) membranes showing promising results with respect to performance and durability [115]. Zhou at al. [116] found that polybenzimidazole (PBI) membranes were advantageous over Nafion® 211 at maintaining capacity. The PBI-based VRFB had a capacity decay rate of 0.3% per cycle, four times lower than that of the Nafion®-based VRFB (1.3% per cycle) due to the extremely low vanadium ion permeability. A cross-linked pyridinium functionalized poly(2,6-dimethyl-1,4-phenylene oxide) (PPO) membrane was fabricated by Zeng et al. [117] to address the issue of low chemical stability for VRFBs. The modified PPO membrane exhibited a superior chemical stability in both the *ex-situ* immersion test and the continuous cycling test. Due to the internal cross-linking networks and the chemically inert polymer backbone, the specific discharge capacity decreased to 80% of the initial value in 537 cycles with a capacity decay rate of 0.037% at a current density of 200 mA cm^{-2}.

In addition to membrane modifications or alternative membranes, membrane thickness adjustment could be another way to obtain extended lifetime for VRFBs. Research has shown that there is an optimum membrane thickness for a given set of properties through which the cell performance can be significantly improved while keeping the membrane material constant [118]. Nevertheless, further efforts are needed to improve ionic conductivity, chemical stability, and ion selectivity of the ion exchange membranes [15].

2.3. Electrode

The electrode is one of the key components of VRFBs, providing active sites for the reaction of redox couples. The essential requirements of a suitable electrode for VRFB applications include electrochemical stability in the operation potential window, chemical stability in highly acidic environments, high oxygen and hydrogen overvoltage, and excellent electrical conductivity for fast charge transfer reactions. The electrode degradation has been found to account for a major portion of the overall performance loss. For example, Derr et al. [119][120] estimated that the overall performance loss for 50 cycles was between 60-75%, 10-55% of which was constituted by electrode degradation, while the remaining losses were accredited to ohmic loss and the imbalance of the electrolyte.

2.3.1. Electrode materials

The history of electrode development for VRFBs has been summarized by Kim et al. [36] with a vivid historical flow chart provided. A variety of carbon materials, including CF, GF, carbon nanofibers, carbon nanotubes, carbon paper, and graphene oxide (GO) have been widely investigated as electrodes for VRFBs [121]. Composite electrodes have also been investigated as bipolar electrodes by blending a variety of carbon materials with polymers. Owing to the high electrical conductivity, excellent chemical stability, three-dimensional network

structure, a large specific surface area, and wide operation potential windows, carbon and graphite felt materials are most commonly used and well-suited for both the positive and negative half-cells in VRFBs [36]. Typical VRFB CF electrode materials have a porosity around 0.8, and a fiber diameter of approximately 10 μm [122].

The electrode reactions take place on the carbon electrodes. In the meantime, the mass transfer of ions/protons and the transport of electrons to/from the active sites of the electrode also occur. The performance of the electrode strongly depends on the properties of the carbon materials used:

- *Chemical stability*: the chemical stability in the acidic electrolyte is closely associated with the lifetime of the electrode.
- *Electrochemical activity*: the electrochemical activity is directly related to the active surface area (which is determined by the surface area of the carbon, pore size distribution, wettability of the carbon, and amount of active sites), affecting charge transfer resistances.
- *Electrical conductivity*: the electrical conductivity influences the cell voltage and energy efficiencies via ohmic resistances.
- *Porosity*: the porosity affects the overall battery system efficiency via the pressure drop through the stack [15].

In general, carbon and graphite electrodes were found to function well under normal charge–discharge cycling conditions with a slow degradation. In varied abused conditions, degradation of the electrode may severely occur.

2.3.2. Electrode degradation mechanisms

Degradation of carbon materials in VRFBs is a complex issue. During the lifetime of the VRFB operation, carbon-based electrodes may suffer degradation from different sources [122]. Likely, a combination of different effects may also be responsible, including material properties and surface chemistry, hydrogen evolution, and mass transport. To gain an overview of factors contributing to electrode stability and degradation in VRFBs, this section summarizes the main degradation mechanisms of the electrode although, so far, there is limited work which takes into account the degradation of the electrodes [123]. Note that the dominant mechanism behind degradation for each case will depend on the operating conditions of the VRFB.

2.3.2.1. Mechanical and thermal degradations

Mechanical degradation often refers to the mechanical stripping of the electrode, which, in turn, brings decreased active surface areas, blocked pores, or increased stresses in the carbon electrode [122]. Kim et al. [36] observed a high rate of mechanical degradation during charging using a carbon cloth (GF-20) electrode material for the VRFB. They attributed this to the low surface area of carbon cloth materials and the flow-by configuration in comparison with the flow-through operation when using CFs as electrodes, thereby limiting the diffusion of vanadium ions and increasing oxygen evolution during charging. Due to mechanical degradation, carbon cloths and papers have not been further considered as electrode materials.

To ensure the long-term durability of VRFBs, the mechanical properties of the bipolar carbon materials must be considered in addition to their chemical stability, electrochemical properties, and electrical conductivity [36]. This explains why significantly thick CFs, with a thickness in the mm range, is usually employed in VRFB applications, unlike the gas diffusion layer, with a thickness in the μm range, in PEM fuel cells. The thick CF serves as an absorber for the stress within the electrode, as well as a connector for the electrical contacts, and thus, safeguards the durability of the electrode. A thicker CF also enhances diffusion lengths, which can reduce the overall resistance [122].

Thermal degradation of the electrode is commonly caused by thermal differences within the electrode. Depending on the load, current densities may be localized, inducing thermal differences within the carbon microstructure

coupled with mechanical/thermal processes during the cell charge–discharge operation. Consequently, mechanical and thermal expansions of carbon may occur due to thermal differences within the electrode. Chemical reaction rates may also be affected. The thermal differences within the electrode could also provoke regional failure in the electrode. Unfortunately, limited work has been done in this field as identifying the causes and understanding the mechanisms is not an easy task [122].

2.3.2.2. Electroless chemical aging

Electroless chemical aging of the electrodes occurs due to chemical reactions of the felts with sulfuric acid or/and with vanadium. Without applying a current or voltage, sulfuric acid, as well as vanadium in the electrolyte, can chemically react with the CFs. This electroless aging, also referred to as chemical aging, was found to be inevitable for all types of CFs commonly used.

So far literature on the aging of VRFBs is scarce, with research on the chemical aging of electrodes being even more so. Derr et al. [124] studied electroless aging of CF electrodes by soaking them in electrolyte for a certain time period at a certain temperature. Without applying any potential, the electrolyte-induced chemical degradation of the felts could then be investigated in both half-cells. Electrochemical impedance spectroscopy (EIS) analysis demonstrated that the aging of the carbon electrodes was associated with the temperature as well as vanadium concentrations. Experiments showed that chemical reactions of the CF with both sulfuric acid and vanadium occur. The three-electrode experiments also confirmed chemical aging under real VRFB operating conditions. X-ray photoelectron spectroscopy (XPS) indicated similar changes to the surface of CFs at both the positive and the negative electrodes. The amount of oxygen functional groups increased while the amount of sp2-hybridized carbon decreased after 8 days of chemical aging. Results also show that the negative electrode is more strongly affected by chemical aging than the positive electrode for a duration of up to 30 days.

2.3.2.3. Electrochemical degradation

The most recognized degradation mode for the carbon electrode is electrochemical degradation, also known as carbon corrosion under acidic environment. For the durability of VRFBs, electrochemical degradation of CF electrodes appears to be a key issue [119]. In the positive half-cell, possible electrochemical reactions include the oxidation of carbon to CO_2 and the oxygen evolution reaction (OER). In the negative half-cell, the hydrogen evolution reaction (HER) competes with the V(II)/V(III) reaction. Almost exclusively, the electrochemical side reactions take place during the charging process, resulting in a decrease in electrochemical surface area (ECSA), as well as activity towards vanadium redox reactions [119].

In the positive half-cell of VRFBs, the carbon electrode is easily corroded because of CO_2 evolution. Under normal conditions, such as during VRFB discharge, the potential is less than 1.4 V and the carbon electrode remains stable. However, during charging, the positive electrode potential is as high as 1.8 V under this high potential; the following reactions may occur at the positive electrode [7]:

$$C + H_2O \rightarrow CO + 2H^+ + 2e^- \quad (13)$$

$$CO + H_2O \rightarrow CO_2 + 2H^+ + 2e^- \quad (14)$$

$$2H_2O \rightarrow O_2 + 4H^+ + 4e^- \quad (15)$$

Due to the change in the surface functional groups or the loss of ECSA at the electrode, these heterogeneous side reactions could cause performance degradation of the electrode. As well, these side reactions consume current densities, and thus may lower the energy efficiency of a VRFB. Also, bubbles formed during the side reactions weaken the effective contact between electrolyte and electrode, reducing the active surface area for redox reactions and disturbing the transport of the reactants. By controlling the applied potential difference, gas

evolution may possibly be supressed. In addition, due to asymmetric internal resistance, local potential and temperature may rise in the cells. As a result, gas evolution in localized regions may occur and the felt electrode corrosion may be expedited due to the decrease in the OER overpotential caused by the increase in temperature [125].

In the negative half-cell of VRFBs, the HER (Equation (16)) has a very strong impact on the performance of the negative electrode. The evolution of hydrogen not only consumes current but also damages the carbon fibers.

$$2H^+ + 2e^- \rightarrow H_2 \quad (16)$$

Side reactions of O_2 and CO_2 evolution were observed by Liu et al. [125] and the corrosion behavior was investigated. When the graphite electrode acts as the positive electrode, it is easily suffered from electrochemical degradation because of CO_2 and O_2 evolution. Using potentiodynamic and potentiostatic techniques, the effects of polarization potential, operating temperature, and polarization time on graphite corrosion were investigated. The results showed that when the anodic potential is higher than 1.60 V vs. saturated calomel electrode at 20 °C, CO_2 and O_2 evolution occurs on the graphite electrode; and when the polarization potential reaches 1.75 V, CO_2 evolution on the graphite electrode can cause intergranular corrosion of the graphite. In addition, they found that functional groups of COOH and C=O on the electrode surface could catalyze the evolution of CO_2, thereby accelerating the corrosion of the graphite electrode.

Derr et al. [119][120] also observed electrochemical degradation of electrodes during cycling experiments and half-cell measurements at various SOCs. As part of their research, XPS revealed that the oxidation of carbon occurred for both half-cells and in a similar manner. SEM observed a peeling of the fiber surface after cycling, resulting in a loss of ECSA. Based on the cycling experiments, it was found that the degradation rate strongly depended on the cycling conditions, including the cut-off voltage and the experiment duration. The higher the cut-off voltage, the faster the electrode degraded. During the cycling experiments, they found that electrochemical degradation was influenced by chemical aging and that electrochemical degradation had a stronger impact on the negative half-cell than the positive half-cell. This implies that the negative half-cell is rate determining for the VRFB and, therefore, modification of the positive carbon electrode does not significantly affect the VRFB performance.

2.3.3. Diagnostic tools for electrode degradation

Considering the significant influence of carbon-based electrodes on the performance of VRFBs, it is very important to understand the factors affecting the performance degradation of graphite electrodes and under which conditions the electrode is severely eroded. Thus, suitable techniques should be identified to ascertain battery degradation mechanisms at the nano-scale of carbon-based electrodes so that proper mitigation strategies could be applied [122].

2.3.3.1. Electrochemical tools

Electrode performance and degradation within a VRFB can be evaluated by electrochemical techniques such as linear sweep voltammetry, cyclic voltammetry (CV), EIS, and cell charge–discharge polarization curves.

Liu et al. [126] studied graphite corrosion and found that in a pure H_2SO_4 solution, graphite started to oxidize at 1.15 V, while in the presence of $VOSO_4$, the onset potential of carbon oxidation shifted to 0.9 V as shown in Figure 5.

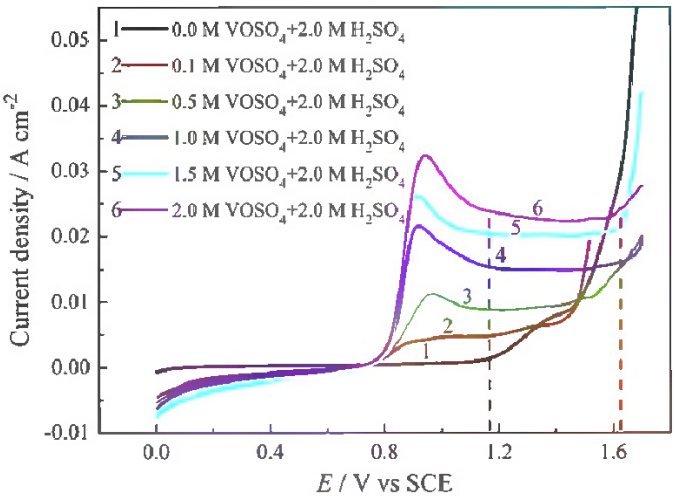

Figure 5 Linear sweep voltammograms of graphite electrodes in different concentrations of $VOSO_4$ with 2 M H_2SO_4 at a scan rate of 5 mV s^{-1} [126] (Reproduced with permission from Elsevier)

CV can be used to identify vanadium redox peaks, compare anodic and cathodic current densities of electrodes, determine the reversibility of the redox couple, evaluate long-term stability, and quantify the ECSA, an important indicator of the electrode performance. Wu et al. [127] studied the performance of GF electrode treated by different methods: thermal treatment, and modified Hummers method. Figure 6 shows the CVs of the GF electrodes. The thermally treated GF exhibited lower oxidation and reduction peak current densities compared with those for the GF treated by the modified Hummers method. These differences were attributed to the formation of oxygen-containing groups on the surface of the GF treated by the modified Hummers method. Increased surface oxygen containing groups improved the surface hydrophilicity, thereby increasing the absorbed water, and further, enhancing the adsorption of vanadium ions on the surface of the electrode and benefiting the electrode reaction. Since the –OH groups provide active sites for V(IV)/V(V) redox reactions, the CE of a VRFB that employs GF treated by the modified Hummers method can be significantly enhanced.

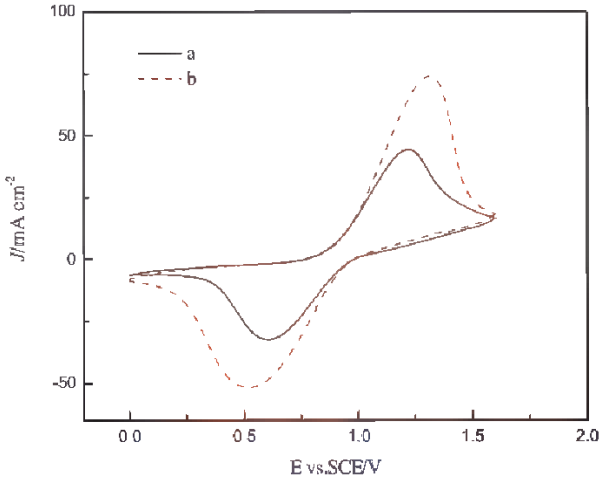

Figure 6 Cyclic voltammograms of (a) graphite felt treated by thermal treatment (b) graphite felt treated by modified Hummers method in 0.5 M $VOSO_4$ + 3 M H_2SO_4 [127] (Reproduced with permission from Elsevier)

EIS is a useful tool to monitor changes in ohmic resistance, double layer capacitance, and charge transfer resistance. The main advantage of EIS over cyclic voltammetry is the low current/voltage that is applied during the measurement, in which case parasitic reactions like the HER can be neglected [124]. Using the EIS results shown in Figure 7, Sun et al. [128] obtained the ohmic, charge transfer, and diffusion overvoltages at the negative electrode of a VRFB. The voltage losses at various flow rates and electrode thicknesses were quantified as a function of current density during anodic and cathodic polarization. Results showed that the diffusion overvoltage was strongly affected by flow rate while the charge transfer and ohmic losses were invariant. A Tafel plot was obtained using the impedance-resolved charge transfer overvoltage; from this, parameters such as the geometric exchange current density, anodic and cathodic Tafel slopes, and corresponding transfer coefficients were then determined.

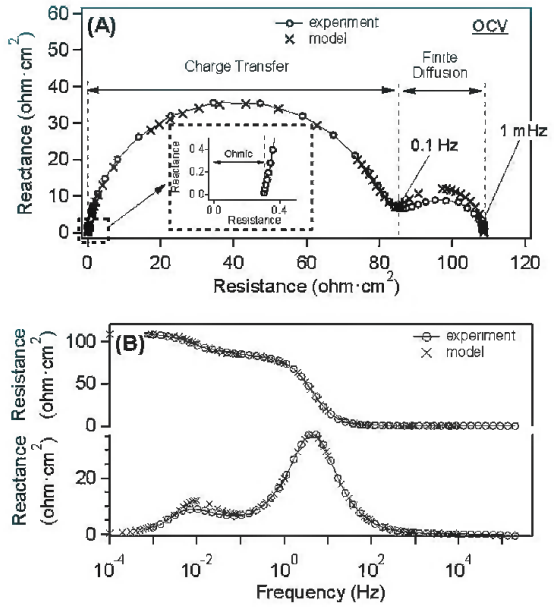

Figure 7 (A) Measured complex impedance spectrum of a V(II)/V(III) single layer anode, at 30 °C and flow rate of 1.5 mL min^{-1}; (B) Frequency dispersion of the resistance and reactance components of the impedance vectors in (A) [128] (Reproduced with permission from ECS)

To evaluate electrode performance, charge–discharge testing is most commonly used. Wu et al. [127] conducted charge–discharge testing of a VRFB cell. Figure 8 presents the charge–discharge curves of two cells with GFs treated by the modified Hummers method (referred to as cell B) and thermal treatment (referred to as cell A) at a current density of 50 mA cm^{-2}. The cell B curve exhibited low charge and high discharge voltage plateaus, thereby achieving high voltage efficiency (VE) because of the increased C–OH groups on the GF surface. The C–OH groups were found to catalyze the redox reaction of V(IV)/V(V) on charge, and both the VE and CE were improved as a result, which was consistent with the CV analysis. For the same reason, the cell B exhibited high charge and discharge capacities.

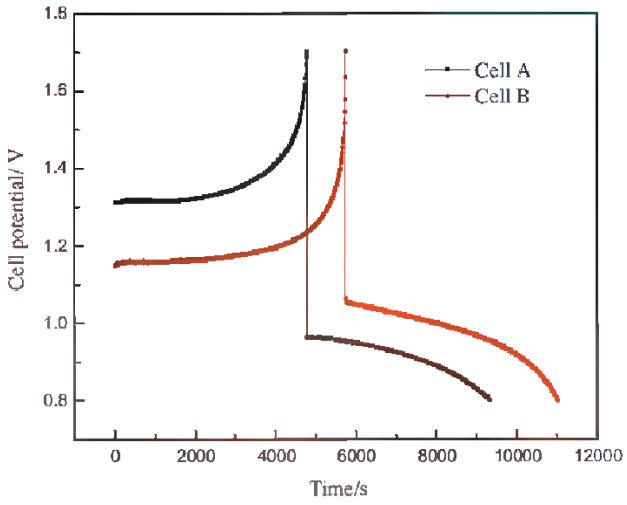

Figure 8 Charge–discharge profiles of cell A (cell employing graphite felt treated by thermal treatment) and cell B (cell employing graphite felt treated by modified Hummers method) at a current density of 50 mA cm^{-2} [127] (Reproduced with permission from Elsevier)

2.3.3.2. Physical tools

This section covers the features of physical methods for VRFB electrode diagnosis. Various techniques have been employed, including mass spectroscopy, XPS, SEM and transmission electron microscopy (TEM) imaging, 3D tomography, and atomic force microscopy (AFM).

Liu et al. [126] studied graphite corrosion using online mass spectroscopy to monitor gas evolution on the electrode. Results showed that CO_2 and CO can simultaneously evolve on the graphite electrode and the evolution of CO and CO_2 on the anodic graphite electrode in 2 M H_2SO_4 was more favorable than that in 2 M H_2SO_4 / 2 M $VOSO_4$. Results also showed that O_2 evolution needs higher anodic polarization (about 1.8 V), and its evolution rate is the highest among O_2, CO and CO_2. At 1.8 V, the electrochemical corrosion of the anodic graphite electrode in 2 M H_2SO_4 was much more severe than in 2 M H_2SO_4 / 2 M $VOSO_4$. It was concluded that the oxidation of V(IV) to V(V) on the graphite electrode impeded the carbon oxidation reaction, and the high concentration of the V(IV) electrolyte was favorable for reducing the electrochemical corrosion of the graphite anode.

Ex-situ XPS has been used to observe variations of the CF surface with respect to changes in the amount of functional groups before and after degradation [124]. The results confirmed that the formation of functional groups on the felt surface is not the main cause for serious changes in the electrical properties of the GF electrodes. XPS has also been used to study overcharged GF [129]. Using XPS, Mohammadi et al. [130] investigated the effect of overcharge on the surface chemistry for three types of GF electrodes. The XPS analysis demonstrated that the overall surface oxygen content of the GFs slightly increased after overcharge with C–OH, –C=O, –COOH and –COOR groups formed.

The morphology and the crystalline structure of the electrode nanoparticles can be studied using SEM and TEM imaging, 3D X-ray tomography, and AFM [125]. Di Blasi et al. [131] presented SEM images of graphite electrodes oxidized at 1.9 V in 2 M H_2SO_4 and 2 M H_2SO_4 / 2 M $VOSO_4$ solutions. Results showed that, in the presence of $VOSO_4$, the oxidized electrode surface is much smoother than that in the absence of $VOSO_4$. This is further evidence that the presence of V(IV) could reduce graphite corrosion.

Micro-computed tomography (CT) or 3D tomography is an exceptional diagnostic tool for monitoring the structural changes in GF electrodes during VRFB operation, providing insights into the nano/micro structure of the electrodes [122]. Reconstructed 3D images of VRFB electrodes revealed that the fiber agglomerates and carbon electrochemically oxidized during battery cycling. Key geometric parameters of the GF could also be captured from the 3D images, allowing the calculation of porosity, characteristic tortuosity, and volume specific surface area. Chakrabarti et al. [122] have shown that 3D imaging has an ability to quantify surface areas, particle sizes, and porosity, identify different phases, and determine tortuosity of the complex electrode structures. Coupled with SEM and XPS measurements, Trogadas et al. [132] successfully elucidated the microstructural and chemical changes of the high voltage VRFB carbon electrode. The results revealed that the corrosion onset of the CF structure occurs relatively early in the VRFB life-cycle, and prolonged operation results in extensive microstructural evolution in the form of agglomerated fiber bundles.

Other physical techniques used to evaluate the electrochemical performance of the GF for VRFBs include Fourier-transform infrared spectroscopy (FTIR), and Brunauer-Emmett-Teller (BET) surface area analysis. FTIR can indicate that the electrochemical oxidation reduces the content of C–O groups and increases the number of –OH and C=O functional groups on the GF surface. The specific areas of the GF samples can be obtained by BET; the increase of specific area can be related to the electrochemical oxidation process [133].

2.3.4. Mitigation strategies for electrode degradation

Although the majority of articles published have aimed at enhancing the electrochemical reactivity of CF electrodes, efforts have also been made to mitigate electrode degradation.

2.3.4.1. Voltage and temperature control

The corrosion current density of graphite electrodes is strongly dependent on the polarization potential and the operating temperature [134]. At a given temperature the corrosion current density increases with higher polarization potential. At a given polarization potential, the corrosion current density increases with the operating temperature. As a result, the CE decreases with increased operating temperature and anodic polarization potential. Therefore, one of the strategies to mitigate electrode degradation is to strictly control the applied potential difference and operating temperature, thereby preventing gas evolution [125].

Since side reactions usually take place during the charging process, the right cut off voltage is very important to prevent gas evolution [119]. The cut-off voltage for charging is commonly set to 1.6 V or 1.65 V to prevent parasitic electrode reactions and battery components degradation [135]. Derr et al. [123] investigated the effect of different cut-off voltages on the degradation of CF electrodes in a VRFB. They chose 1.65 V and 1.8 V as the cut-off voltages to compare hydrogen evolution on the negative side and CO_2 evolution on the positive side. For the positive half-cell, the risk of CO_2 evolution increased with increasing cut-off voltage. However, the higher cut off-voltage did not increase the risk of evolving hydrogen on the negative side. In general, the higher cut-off voltage lead to a higher rate of degradation. The main reasons for the loss of performance were the imbalance of the electrolyte and the degradation of the CF electrode. By exchanging electrolyte, the electrode degradation was proven to be responsible for 55% and 25% of performance loss for the 1.65 V and the 1.8 V cut-off voltage, respectively.

2.3.4.2. Electrode modification

There are numerous publications investigating the modification of carbon/graphite felt [136]. A variety of modification methods have been reported to improve the electrochemical activity of electrodes, such as nitrogen doping, integration of functional groups, surface modification (e.g., Bi, PbO_2, ZrO_2 etc), and various thermal or other treatments (e.g., ammonium, Fenton's agent, H_2O_2 etc.). These approaches of electrode modification aim to promote electrochemical activities of the electrode. Some publications focus on improving the positive half-cell electrode because the electrochemical kinetic limitations of VRFBs are related to the V(IV)/V(V) reaction while

other publications deal with the negative electrode due to the fact that this electrode limits the CE of the battery. In general, most of the reports describe improvement in electrochemical activity of the electrode. Regarding long-term stability or calendar life, limited research has been conducted.

Shi et al. [137] studied nitrogen-doped graphene as the positive electrode in a VRFB. The electro-catalytic activity of the NGS-20 modified electrode was markedly enhanced compared to the RGO-20 for the V(IV)/V(V) redox couple reactions. Among the four nitrogen species, the quaternary-N was more stable in the acidic environment and more likely served as active sites for enhancing electrochemical catalytic activity as well as cycling stability. Huang et al. [138] demonstrated the preparation of N, O dual-doped CF as electrodes in VRFBs. N_2 and O_2 plasma were employed to treat the CF, introducing nitrogen and oxygen atoms into the CF to result in improved electrocatalytic activity and enhanced interaction of CF and electrolyte during battery operation. The energy efficiency of the VRFB was improved from 65% (pristine) to 78% (doped) at a current density of 50 mA cm^{-2} with excellent cycling stability.

Kim et al. [139] prepared a new type of CF with oxygen-rich phosphate groups through direct surface modification with ammonium hexafluorophosphate (NH_4PF_6). Owing to the superior catalytic effects of the oxygen-rich phosphate groups, the electrochemical reactivity of the CF towards the V(IV)/V(V) and V(II)/V(III) redox reactions were shown to be effectively improved. Undesirable hydrogen evolution could also be suppressed by minimizing the V(II)/V(III) redox overpotential in the anolyte. In terms of electrode durability, cell-cycling tests were conducted. The electrode demonstrated good stability within the VRFB with improved energy efficiencies. Estevez et al. [140] introduced tunable oxygen functional groups onto the surface of a GF using O_2 plasma followed by H_2O_2 treatment. Electrode cycling performances of the VRFB with this optimized GF electrode at different current densities showed no apparent fading after 50 cycles at the same operating current density.

Wei et al. [141] developed a GF electrode with a copper nanoparticle deposition for VRFBs. It was found that the copper catalyst enabled a significant improvement in the electrochemical kinetics for the V(II)/V(III) redox reaction. Moreover, the tested battery showed good stability during the cycle test. A recent study described a new Ni-plated CF and the effect of plating thickness on the mechanical, electrical, and morphological properties of the electrode. Experimental results showed that the area specific resistance drastically reduced under 40% compression, while the stress-strain curve, residual strain, and porosity remained unchanged [122]. Bismuth nanoparticles have also been reported to have a very positive effect on the performance of a rayon-based GF for the negative electrode of a VRFB [142]. The reversibility of the V(II)/V(III) redox reactions and the long-term cycling performance of the electrode were significantly enhanced. This was explained by the fact that Bi nanoparticles favor the formation of BiHx, an intermediate that reduces V(III) to V(II) and, therefore, inhibits the competitive hydrogen formation. Zhou et al. [143] synthesized a series of ZrO_2-modified GF (ZrO_2/GF) electrodes with varying ZrO_2 content via an immersion-precipitation approach. In addition to the improved electrochemical activity and reversibility toward the V(IV)/V(V) and V(III) to V(II) redox reactions, the cycle tests demonstrated that the ZrO_2/GF electrodes exhibited outstanding stability with negligible decay after 200 cycles.

In terms of surface treatment, Gao et al. [144] investigated the effect of Fenton's reagent on the GF performance. The GF treated with Fenton's reagent containing H_2O_2 exhibited excellent electrochemical activity for the V(IV)/V(V) redox reaction and the treated GF electrode possessed higher stability and efficiency than the untreated one. Through thermal treatment in a tube furnace, Kabtamu et al. [145] modified GF electrodes. The water-activated GF electrode exhibited high electrochemical activity and reversibility for the V(IV)/V(V) redox reaction; this is because numerous oxygen-containing functional groups, such as –OH groups, are produced on the surface of GF fibers. Stability tests revealed no apparent decay in efficiency after 30 cycles, implying that the thermally treated electrode had high stability during the redox reactions under highly acidic conditions.

With respect to electrode modifications to improve performance, the aforementioned methods are mostly to modify raw felts into electrodes with individual unique features. Another possible approach could be the combination of currently recognized modification methods. For example, GFs can be treated by thermal or chemical methods to create a hydrophilic surface before employing other techniques such as metallic-, graphene-, or polymer-based modifications [146]. Note that surface modified carbonaceous material usually exhibits excellent performance in the initial cycles; however, the modifications are not sustainable when prolonged cycling tests are performed. Hence, future research needs to be focused on the long-term activity of electrocatalysts for improved cycling life [15].

2.4. Bipolar plates

BPs are important elements within the VRFB, providing electrical conductivity and physical separation of adjacent cells. As BPs are in direct contact with acidic electrolytes that contain vanadium species in different oxidation states, corrosion of BPs can occur, especially, under extended overcharge conditions. Therefore, BP corrosion can be a major issue for long term stability of VRFBs.

2.4.1. Functionalities and types of the bipolar plates

BPs have several functions in a VRFB: (1) physically separating adjacent cells from each other; (2) electrically connecting cells in series, and (3) providing structural supports for the VRFB stack. Therefore, the main requirements of suitable BPs are high chemical stability in the electrolyte, low electrical resistance/good electrical conductivity, and strong mechanical properties.

As graphite sheets offer higher electrical conductivity, they are conventionally used as the BPs for VRFBs, giving desirable high power density of the stack. However, the graphite plates are costly among the VRFB components due to the fabrication of thin graphite plates which are prone to breakage during machining or handling [147]. As a result of the lower cost and superior mechanical properties, a number of VRFB manufacturers have used metal BPs and composite BPs in their low cost stack designs to overcome the problems of graphite BPs. Table 4 summarizes different types of BPs and their advantages and disadvantages [7]. Carbon composite BPs have had the most attention in recent research with the advantage of lower cost and reduced weight. However, the challenge has been to achieve good conductivity while maintaining mechanical strength. Conductivity in carbon-polymer composites is linked to carbon fillers (such as carbon black or carbon fiber) which take up to 20-60 weight% in the composite to have sufficient conductivity [148][149][150][151]. To increase the conductivity of the composite BPs, several surface treatment methods have been applied. Plasma surface treatment of the carbon composite BP was reported to increase the electrical conductivity by 70% [152] but the high cost and insufficient low conductivity still remained as an issue. Surface coating of the carbon composite BP with graphite was also reported to increase electrical and chemical stability [147].

Table 4 Comparison of various types of bipolar plates [7]

Type of BP	Advantages	Disadvantages
Graphite BPs	• High conductivity • Low corrosion	• High cost in machining • Vulnerable to breakage
Metal BPs	• High conductivity • Mechanically strong	• Au or Ti coating needed • High cost and low productivity
Carbon composite BPs	• High mechanical strength • Low weight • Low cost	• High electrical contact resistance • Lower conductivity

2.4.2. Bipolar plate degradation mechanisms

2.4.2.1. Electrochemical corrosion

Electrochemical corrosion of the BP is mainly caused by the electrical potential between the acidic electrolyte and the BP. According to recent studies, the most important factor affecting the electrochemical corrosion of BPs in VRFB stacks is gas evolution, including H_2, O_2, CO, and CO_2. These gases are induced by the electrical potential in the VRFB stack in the form of side reactions, producing crucial defects on the surface of the BPs or degrading the coating layer of the BPs.

In the positive half-cell, oxidation reactions of carbon, from either the graphite BP or the carbon black filler material in carbon composite BPs, can take place above the critical half-cell voltage of E_{cr} = 1.6 V [126][153], particularly when the battery is being overcharged. The oxidation of the graphite or carbon black filler material through side reactions during overcharge is shown in Equations (13-14). These reactions lead not only to the increase in resistance but also to CO_2 formation resulting in delamination and destruction of the composite matrix.

In a VRFB cell, the potential difference is approximately 1.4 V, which may electrolyze water into oxygen and hydrogen (Equations (15-16)) during the VRFB operation. Under certain circumstances, electric current may go through the electrolyte flow path. As a result, it generates a potential difference higher than 1.4 V on the BP of VRFBs. The newly generated oxygen from electrolysis is very active and easily combines with graphite. Sulfuric acid in the electrolyte is also a very strong oxidizing agent, accelerating the reaction. As for hydrogen evolution, the gas generation rate is particularly severe when metal coating is involved. To increase the corrosion resistance and conductivity, the metal substrate is usually coated with corrosion-resistant metals, such as gold or titanium [154]. However, this coated metal might catalyze the HER in the negative half-cell, competing with the anodic reaction and not only leading to the loss of battery efficiency but also causing bulges and delamination on the surface of BPs during gas evolution.

Electrochemical corrosion of BPs should be investigated based on the types of BPs and the properties of the coating layer. Kim et al. [155] estimated the electrochemical corrosion of composite BPs, on which expanded graphite was coated to decrease the interfacial contact resistance of the carbon composite. Results showed that damage to the coating layer of the composite BP during actual operating condition can reduce durability of the composite BP.

Choe et al. [156] investigated the graphite coating's durability on a carbon/epoxy composite BP in vanadium electrolyte with highly concentrated sulfuric acid. Under electrochemical corrosion, they measured the mass loss of graphite with respect to time. Results showed that gas evolution weakened the van der Waals force between the graphene layers, causing electrochemical exfoliation of the graphite. The degradation of the graphite coating increased the resistance of the BP, thereby decreasing the efficiency of the VRFB. In addition, the delaminated graphite polluted the electrolyte and filled the pores of the CF electrodes, which, in turn, increased the pumping loss.

Liu et al. [157] also investigated the corrosion behavior of a carbon–polythene composite BP and the effect of corrosion on its mechanical strength. They observed erosion of the composite BPs due to gas evolution (CO_2, CO, and O_2) when the anodic polarization potential was above 2.0 V in 2 M $VOSO_4$ in 2 M H_2SO_4. The results showed that oxygen functional groups (C=O and O=C–OH) were formed on the surface of the BPs. Also on the surface, bulges and delamination were observed due to gas evolution, resulting in a decrease in mechanical strength and electro-conductibility of the BPs. The conductive network of BPs can also be destroyed, leading to similar declines.

Other factors influencing corrosion include [7] :

- Graphite composition
  - Composition
  - Matrix microstructure
  - Technique adopted for preparing the composite
  - Chemical and physical homogeneity of the BP surface
- Environment
  - Hydrogen-ion concentration (pH) in the solution
  - Specific nature and concentration of the other ions in solution
  - Localized concentration gradients at high SOC
  - Dead zones (poor fluid distribution) can lead to depletion zones causing high localized overvoltage zones
  - Cyclic stress (corrosion fatigue)

2.4.2.2. Chemical/electroless aging

Up to now, most published papers about BP corrosion have focused on aging due to cycling. In reality, aging not only occurs during battery charge and discharge but also during electroless rest conditions [157].

Satola et al. [158] studied the influence of SOC on the calendar aging of BPs. Graphite-polypropylene BPs were immersed in positive and negative vanadium electrolytes at 0%, 20%, 80% and 100% SOC for 30, 90 and 190 days. During the immersion, H_2 gas evolution was observed on the surface of BPs in the anolyte. After electroless aging, no significant changes were noticed in the surface morphology and electrical conductivities of BPs. However, the catholyte was found to affect the wettability of BPs, and both sulfuric acid and V(IV) ions that were adsorbed in the pores motivated the oxidation of the graphitic compounds. Further penetration of water and vanadium ions into the graphite structure of the BP was then promoted. The penetration of V(IV) species in the bulk of BPs could be critical for chemical aging, especially when the electric potential difference is increased. To maintain the lifetime of the BPs, storage at a fully charged electrolyte state for prolonged periods of time should be avoided. Nevertheless, further investigation under operating conditions is needed to fully understand aging effects.

2.4.2.3. Oxidation caused by shunt current

There are two types of current flow pathways inside the VRFB stack, the main current path and the shunt current path [159][160][161], as shown in Figure 9 [147]; these can also be referred to as through-plane current pathway and in-plane current pathway, respectively. Along the main current path, electric current flows from cell to cell within the active area of the VRFB stack; this involves passing through the BPs, the CF electrodes, the electrolyte, and the proton exchange membrane. Along the shunt current path, the electric current flows in the direction of the flow channel between cells and is supported by the conductivity of the electrolyte. Shunt currents are not limited to single stacks; they also exist in battery systems consisting of several stacks.

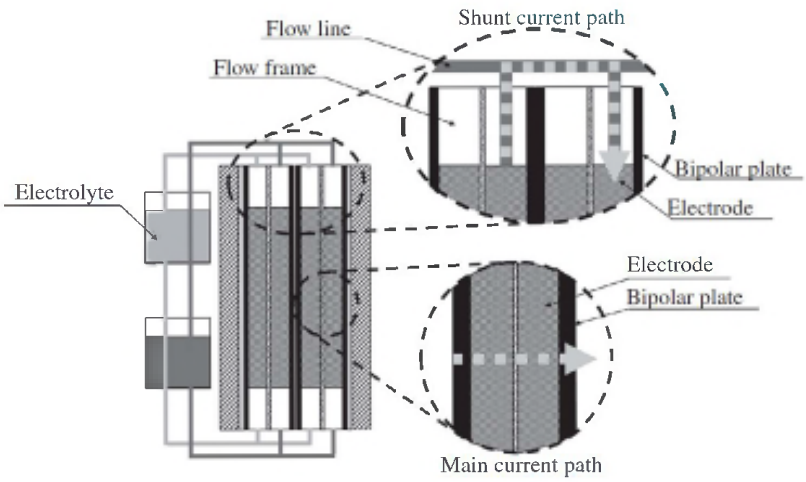

Figure 9 A schematic drawing of the main current path and the shut current path in the VRFB stack [147] (Reproduced with permission from Elsevier)

The total resistance, $R_{total,}$ of a unit cell in the main current path can be written as Equation (17) and the total resistance of a unit cell in the shunt current path can be written as in Equation (18) [147]:

$$R_{total} = R_M + 2R_{BP} + 2\frac{1}{\frac{1}{R_{BP/CF}+R_{CF}}+\frac{1}{R_E+R_{E/BP}}} \quad (17)$$

$$R_{shunt} = 2R_{BP} + 2R_{E/BP} + R_E \quad (18)$$

where R_M represents the equivalent resistance of the membrane; R_{BP}, R_{CF}, and R_E represent the resistance of the BP, CF electrode, and electrolyte, respectively. $R_{E/BP}$ represents the interfacial contact resistance between the electrolyte and the BP.

It has been reported that the shunt current might be the driving force behind the corrosion process whereas the main current is less dominant [155]. In the main current flow path, most charges exist in the membrane due to the high electrical potential since the membrane resistance is relatively high among other components; the electrical potentials between the electrolyte and BPs can be negligible. Therefore, the main current path does not dominate the electrochemical corrosion of the BP. In the case of the shunt current path, the electrical potential between the electrolyte and BPs is relatively high compared to that in the main current path. As a result, the shunt current becomes a dominant factor for the electrochemical corrosion of the BP, shortening the life of BPs, affecting the performance of the VRFB, and decreasing the energy transfer efficiency due to an internal self-discharge [162].

In-plane shunt current can be induced by local potential differences in the VRFB cells. Depending on the concentration of the species in the electrolyte, which is related to the SOC of the electrolyte, the electrical potential varies from 0 V to 1.6 V based on the Nernst equation. The non-uniform electrolyte flow and non-uniform electrolyte SOC in the VRFB cells may induce electrical potential differences, which in turn inflicts the in-plane current of electricity flowing along the BPs. In-plane potential differences can be increased to reach as high as 1.6 V [155].

There are several publications regarding shunt currents, mostly focusing on creating models rather than conducting experimental investigations. Fink et al. [162] compiled a detailed understanding of shunt currents in

a VRFB stack and presented shunt current effects for different cell designs and cell counts. They built a stack with an external hydraulic system, allowing them to switch shunt currents on and off. Thus, the contributions to self-discharge could be distinguished between cross-contamination and shunt currents, and the loss of current could then be determined by charge conservation measurements. Results showed that, in a classical frame design, the increase in the number of cells in a stack clearly led to the increase in shunt currents. Based on the circuit analog method, Xing et al. [161] proposed a stack-level model to investigate shunt current loss within the VRFB. Results showed that the percentage of shunt current loss within the total coulomb loss was less than 17%. The stack shunt current of VRFBs was also studied by Yin et al. [23] with both experiments and 3D simulations. They calculated voltages and electrolyte conductivities based on electrochemical reaction distributions and SOC values, and estimated coulombic loss based on shunt current and vanadium ionic crossover through the membrane. According to their model, the number of cells in the stack played an important role in the loss of shunt currents. This model could also be used to optimize the VRFB stack manifold and channel to improve system efficiency.

2.4.3. Diagnostic tools for bipolar plates degradation

2.4.3.1. Property measurements

The performance of BPs greatly depends on the specific type, and therefore the specific properties, of the BP. The degradation mechanism(s) and degradation rate of BPs are also associated with these properties, including permeability, mechanical properties, and electrical properties.

During the fabrication of composite BPs, the solution casting method is usually used. Bubbles or defects could form during the curing process. By measuring permeability, the reliability of the BP could be verified. To measure the gas permeability of BPs, Nam et al. [163] used a 2-chamber device separated by the BP sample. Air pressure of 0.2 MPa was applied to chamber 1 and the pressure in chamber 2 was observed for 100 h. The gas permeability of the BP could then be calculated. Choe et al. [156] also measured the permeability of various graphite foils via water vapor instead of air. The following standard equation was used to calculate the permeability:

$$Permeability\ coefficient = \frac{WVTR}{P_w} b \quad (19)$$

where WVTR is the water vapor transmission rate, P_w is the pressure difference across the specimen, and b is the thickness of the specimen.

As BPs for VRFBs have to provide strong support to the thin membrane and the CF electrode as well as withstand the high compression pressure of the stack over a long cycle life, BPs must have strong mechanical properties. The mechanical properties of the BP can be measured by a pull-off test using a universal testing machine. The pull-off tension tests can observe the elongation [164] and determine the Young's modulus, Poisson's ratio, and tensile strength of the BP.

The resistance of the BP, which affects the ohmic loss in a stack, is an important factor that contributes to the efficiency of VRFBs. The total resistance of the fabricated BP can be measured using the four-point probe method in the through-plane. By placing a BP specimen between two CF electrodes, assembling this between two gold-plated copper plates, and applying an electrical current to the testing setup, voltage can then be measured under different compression pressures to calculate the resistance [156]. The areal specific resistance (ASR) of the BP specimen, R_{ASR}, can be calculated by subtracting R_{sub} from R_{total}, shown in Eq. (20). The electrical resistance, R_{total} and R_{sub} are defined in Eqs. (21) and (22), respectively.

$$R_{total} = R_{electrode-felt} + R_{felt} + R_{felt-BP} + R_{BP} + R_{felt-BP} + R_{felt} + R_{electrode-felt} \quad (20)$$

$$R_{sub} = R_{electrode-felt} + R_{felt} + R_{electrode-felt} \quad (21)$$

$$R_{ASR} = R_{total} - R_{sub} = R_{BP} + R_{felt} + 2R_{felt-BP} \quad (22)$$

where $R_{electrode\text{-}felt}$ is the interfacial contact resistance between the electrode and the CF, R_{felt} is the bulk resistance of the CF, $R_{felt\text{-}BP}$ is the interfacial contact resistance between the CF and the BP specimen, and R_{BP} is the bulk resistance of the BP specimen [163]. Using the same four point probe equipment, Satola et al. [158] measured the electrical resistivity with a RM3-AR test unit. Six measurements were performed at different locations on the surface of the BPs and the specific electrical conductivity was then calculated.

2.4.3.2. Ex-situ corrosion tests

Corrosion tests of graphite-based BPs

For investigating the corrosion of graphite-based BPs, tests can be done *ex-situ* using a traditional three-electrode set-up. Komsiyska et al. [165] used this set-up to investigate graphite-based BP corrosion in V(IV)/V(V) + H_2SO_4 electrolyte. The following conditions were used in their tests:

- Electrolyte:
  - 1.5 M V(IV)/V(V) (SOC ~80%) in 2.0 M H_2SO_4
  - 1.5 M V(IV)/V(V) (SOC ~80%) in 2.0 M H_2SO_4 + 2.0 M Cl^-
- Accelerated aging test:
  - 30 repeated linear sweeps @ 2 mV s^{-1}
  - Cycling to potentials from 0.9 V to 2.0 V vs. standard hydrogen electrode (SHE)
  - Conducting EIS every 10th scan

It was observed that:

- At voltages higher than 1.6 V vs. SHE, oxidation reactions occurred followed by oxygen gas evolution;
- Continuous sweeping up to 2.0 V vs. SHE caused dramatic degradation at the surface and the bulk of the BP;
- Presence of Cl^- ion in the electrolyte seemed to suppress the aging of BP at very high overvoltages (2.0 V vs. SHE);
- Cl_2 evolution started at 1.15 V vs. SHE which could reduce CE of the VRFB.

Komsiyska et al. [165] proposed processes for the oxygen evolution reaction, chlorine evolution, and CO_2 formation on the subsurface of the BP in the presence of H_2SO_4 and HCl electrolyte that account for the corrosion of graphite BPs.

Using a traditional three-electrode set-up, Kim et al. [147] conducted *ex-situ* tests to investigate the corrosion of graphite-based composite BPs. To best reflect the corrosion under operating conditions, they mimicked the actual operating conditions of a VRFB. The applied voltage was 1.6 V and the applied current was 20 mA cm^{-2}. The shunt current in the VRFB stack is normally about 2% of the main current [161], or 1.6 mA cm^{-2} for a unit cell that operates at a main current of 80 mA cm^{-2}; therefore, the electrochemical corrosion test was performed with a current density 12.5 times higher than the actual working condition. In their tests, they compared the ASR before and after the tests to observe the corrosion effect. Due to the electrochemical corrosion, the change of ASR as a function of the thickness of the carbon fabric/graphite hybrid composite BPs can clearly be seen. Basically, the thicker the coating layer, the greater the increase in ASR.

To investigate the aging of commercially available graphite-polypropylene BPs, Satola et al. [166] also conducted corrosion tests in a three-electrode electrochemical cell with catholyte (V(IV)/V(V)) at different SOCs. After 3000 cycles in the catholyte at high SOC, the BPs show an increase in double layer capacitance, roughness, and open pore volume. The aging effects are ascribed to oxidation and corrosion of the surface.

Corrosion tests for metallic BPs or BPs with metallic coating

Caglar et al. [154] employed a three-electrode set-up, similar to the one presented in Komsiyska et al. [165], to investigate the HER and electrochemical stability in the anolyte for conductive polymer composite and coated metal BPs. For hydrogen evolution, potentiodynamic measurements were conducted. Detailed procedures are as follows:

1) Potential sweep from OCV in the cathodic direction until reaching -500 μA cm^{-2} using a sweep rate of 5 mV s^{-1};
2) Continue the potential sweep in the anodic direction until reaching +500 μA cm^{-2} using a sweep rate of 5 mV s^{-1};
3) Sweep back in the cathodic direction until 0.3 V vs. OCV.

Results showed that Ti-DLC material with a thickness of 0.5 μm exhibited the highest corrosion current and a much earlier start of the HER in the anodic sweep.

In terms of electrochemical stability, the same research team conducted a potential cycling test for 200 cycles between -0.6 V and 1.4 V vs. normal hydrogen electrode and presented the stability testing results of titanium-coated BPs with different thicknesses. The results showed that the thickness of a coating does not necessarily correlate with its electrochemical stability. For example, the 3 μm coating corroded much faster than the 2 μm coating, suggesting that another effect such as pinhole distribution and size must be part of the degradation of the coatings on the metallic substrate.

It should be noted that *ex-situ* tests are often accompanied with post-mortem physical characterizations such as SEM, TEM, XPS, XRD, FTIR, and X-ray CT.

2.4.3.3. In-situ corrosion tests

Thus far, the *in-situ* tests for BPs have been conducted only with single cell tests through charging/discharging operation followed by calculation of energy efficiency and discharge power density [147][154].

Kim et al. [147] studied the durability of their carbon/graphite hybrid BPs by performing five charge–discharge cycles at one single constant current density of 80 mA cm^{-2} with the voltage being controlled within 1.2-1.6 V, from which the efficiencies were averaged. It was concluded that, due to the low surface hardness of the graphite coating layer on the carbon/graphite hybrid BP in comparison with the conventional BP, the energy efficiency of the unit cell composed of the hybrid BP was 86%, 6% higher than the case of the conventional graphite BP. Note that the *in-situ* tests have to be in conjunction with *ex-situ* tests including area specific resistance as a package of diagnostic tools.

Caglar et al. [154] evaluated the VRFB single cell via galvanostatic charge–discharge tests using metal-coated BPs with an active area of 40 cm^2. The applied constant current varied from 1 to 4 A and the obtained voltage was controlled within 0.8 to 1.6 V; they then calculated the discharge power density (mW cm^{-2}) as well as energy efficiency with the following equations (Equations 23-25).

$$Energy\ Efficiency = \left(\frac{W_{out}}{W_{in}}\right) \times 100\% \quad (23)$$

$$W = \int U(t) \times I(t) \times dt \quad (24)$$

$$P_{discharge} = (\frac{1}{t}) \int U(t) \times I(t) \times dt \quad (25)$$

where W_{out} is the discharge energy, W_{in} is the charge energy, U(t) is the voltage since time t=0, I(t) is the applied current since t=0, and $P_{discharge}$ is the discharge power.

Results showed that the capability of their investigated BPs working at higher current densities was a sign for good electrical conductivity especially in the through-plane direction. As well, the superior discharge power density values were indicators of favorable surface structure for vanadium redox reactions and increased reaction rates; although the main redox reactions take place on the graphite electrode, BPs are still responsible for a part of those reactions.

2.4.4. Mitigation strategies for bipolar plate degradation

2.4.4.1. BPs with high corrosion resistance

To ensure long cycle life, recent studies on BPs are still focused on designing BP substrates with good corrosion resistance by either developing novel low cost composite BPs or novel methods to manufacture BPs.

Carbon/epoxy composite BPs are an ideal substitute for graphite BPs. Lee et al. [167] developed an innovative manufacturing method that exposed carbon fibers on the surface of the carbon/epoxy composite BP, preventing the formation of a resin-rich area. The developed method considerably decreased the ASR of the carbon composite BP without an expanded graphite coating. To cut down the manufacturing cost, Chang et al. [168] designed and fabricated an integrally molded BP; however, real testing in a VRFB was not performed.

To reduce the interfacial resistance of composite BPs, Choe et al. [156] coated composite BPs with pyrolytic graphite and expanded flake-type graphite. It was found that the pyrolytic graphite had higher durability because its graphene sheets were crystallized in a planar direction with a highly oriented structure. It was also found that the pyrolytic graphite-coated BPs showed no degradation after 20 h of single VRFB cell testing while the conventional BPs demonstrated partial delamination of graphite, indicating that the newly designed BP was more durable.

Yang et al. [164] proposed a novel design of BPs for VRFBs by injecting molten polyethylene into micropores of CF. The results showed that the newly designed BPs had higher conductivity, improved mechanical strength, and better overall electrochemical performance and voltage efficiency compared to that of conventional BPs. These improvements were attributed to the conductive CF network structure attained by the molding method used to prepare the novel BP, which affectively lowered the overall resistance of the BP.

2.4.4.2. Other methods

As aforementioned, the electrical potential between the electrolyte and the BP is the main cause of the electrochemical corrosion of the BP, and gas evolution induced by the electrical potential greatly affects the electrochemical corrosion of BPs in VRFB stacks. To prevent corrosion, it is very necessary to greatly improve the uniformity of the BPs in the VRFB stack in order to strictly control the potential applied to all areas of the BP.

For metallic BPs, a metal-doped coating with corrosion-resistance and conductive properties can be applied on the metallic substrate [154]. As the electrochemical behavior of the coated metal is closely related to the HER, the selection of doping metals with suitable hydrogen evolution overpotential is crucial for the coating layer.

To enhance the electrochemical durability of carbon composite BPs in VRFBs, Kim et al. [155] developed a surface crack closing method for the expanded graphite coating layer by performing compressive tests on the

expanded graphite. Under compressive pressure, permanent deformation of the expanded graphite on the surface can occur to close the micro cracks generated. Based on the ASR test results, the required compaction pressure for the micro crack closing process was greater than 12 MPa. SEM observation of the specimens revealed that the micro cracks were effectively removed by the surface crack closing method, thus, efficiently increasing the durability of the carbon composite BPs.

3. Degradation of VRFB cells

VRFB cell degradation is demonstrated by performance decrease and capacity decay. Aside from the components degradation, VRFB degradation at the cell level is mainly due to imbalanced electrolyte and imbalanced SOC caused by vanadium crossover, water crossover, side reactions at both sides and V(II) oxidation by air at the anode side [95][169].

3.1. Degradation mechanisms at cell level

3.1.1. SOC imbalance

Vanadium species with different oxidation states have different diffusion coefficients and, therefore, their crossover rate from one side of the cell to the other is different, resulting in one side with a high V concentration (cathode side) and the other side with a low V concentration [95][169]. Luo et al. [170] studied the capacity decay of a VRFB and found that both the imbalanced vanadium active species and asymmetrical valence of vanadium ions in the catholyte and anolyte were the main cause for the decay. Although the same amount of electricity is charged/discharged to/from cathode and anode during the cell operation, the ratio of V(V) over total V in catholyte is not the same as the ratio of V(II) over total V in anolyte. This is attributed to the fact that the total V in the catholyte is different from that in the anolyte. During cycling, the SOC range in the catholyte becomes narrower while in the anolyte it becomes wider. The increased SOC range of the anolyte corresponds to the lower concentration of V(III), resulting in an increase in concentration polarization for the charge process, while the decreased SOC range in catholyte also arouses an increase in concentration polarization for the discharge process.

Imbalanced SOC can also be caused by side reactions at both electrodes. At the anode, the HER may occur and V(II) oxidation by air may lead to the consumption of electricity and active species. At the cathode, oxygen evolution may occur consuming electricity. Wei et al. [171] studied hydrogen evolution in a VRFB using both *ex-situ* (traditional three-electrode cell) and *in-situ* (during VRFB operation) methods. It was found that the HER rate was strongly affected by temperature and that H_2 evolved even at low SOC, contrary to the common concept of the HER occurring at high SOC. Macroscopic observations showed that, at the negative electrode, H_2 bubbles covered the active sites for the V(II)/V(III) redox reaction. At the positive side, O_2 corroded the electrode surface leading to the formation of oxygen containing functional groups.

3.1.2. Electrolyte imbalance

Ngamasai and Arpornwichanop [172] studied the effect of electrolyte imbalance on the energy capacity of a VRFB. They analyzed the electrolyte imbalance during VRFB operation and calculated the capacity loss at different levels of imbalanced electrolyte. The results showed that the impact of electrolyte imbalance on the capacity and the overall capacity loss can be estimated when the imbalance is detected.

Electrolyte imbalance may be caused by water crossover, which can lead to volume change of the anolyte and catholyte during VRFB operation. However, there are discrepancies regarding water crossover within the literature. Sukkar and Skyllas-Kazacos [100] studied water transfer across different membranes with electrolytes at different SOCs during self-discharge. It was found that the SOC affects the water crossover direction and

crossover amount. Significant water transfer from the catholyte to the anolyte was found when the VRFB was over-discharged; insignificant water transfer was reported at higher SOCs. Sun et al. [96] observed different volume change patterns with respect to CEMs and AEMs. With Nafion® 115, significant volume change (catholyte volume increase, and anolyte volume decrease) was observed in the first several cycles and then volume remained constant. For AEM, in the first 50 cycles, catholyte volume increase and anolyte volume decrease occurred; after 64 cycles, volume change in the opposite direction was found (Figure 10). During cycling, Luo et al. [170] observed catholyte volume increase and anolyte volume decrease with Nafion® 115 as well. While significant volume change was found in the first 5 cycles, slow, continuous volume change was observed in the remaining 195 cycles. Wang et al. [173] found that volume change during the VRFB cycling never stopped, and after 244 cycles using Nafion® 115 membrane, the anolyte tank became empty. Overall, with CEMs, catholyte volume increased and anolyte volume decreased during cycling according to Wang et al.

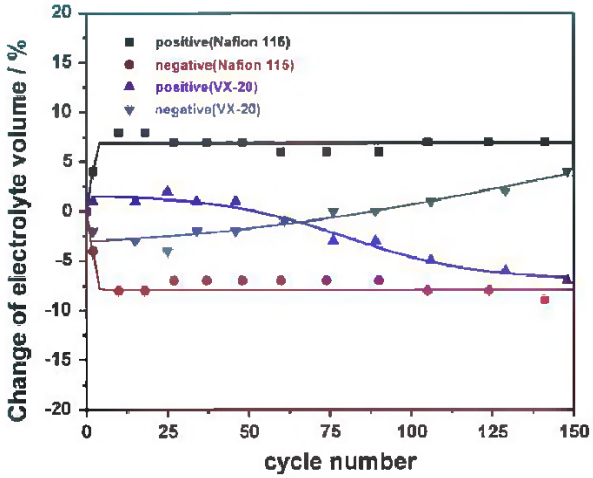

Figure 10 Change of electrolyte volume in the positive and negative half-cells during cycle process when using Nafion® 115 or VX-20 as membrane [96] (Reproduced with permission from Elsevier)

3.2. Mitigation strategies for cell degradation

3.2.1. Mitigation of SOC imbalance

Several methods have been developed to mitigate the SOC imbalance. Whitehead and Harrer [174] developed a method to mitigate the SOC imbalance by using the evolved H_2 to reduce V(V), where a single tank with two compartments was used and a carbon paper coated with catalyst (Ir, Pt, or PtRu) was placed at the catholyte surface. The goal of the catalyst was to catalyze the following reaction; PtRu was found to be the best catalyst.

$$VO_2^+ + 1/2H_2 + H^+ \rightarrow VO^{2+} + H_2O \quad (26)$$

Figure 11 shows the concept of the proposed catalytic rebalance approach. In this way, the SOC of both sides can be rebalanced. Although this method works to rebalance the SOC, it is impractical in commercial applications.

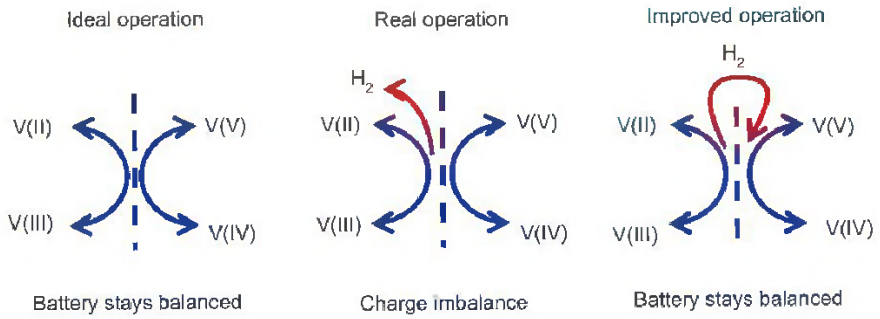

Figure 11 Schematic representation of the proposed catalytic rebalance concept [174] (Reproduced with permission from Elsevier)

The SOC can also be rebalanced by the addition of organic materials to adjust the catholyte average oxidation state (AOS). For long term operation, V(V) accumulation can result in higher AOS in catholyte. Extra V(V) can be reduced by organic materials to restore the original AOS. For example, UET applied fructose to rebalance the catholyte AOS, restoring the electrolyte energy density [175].

3.2.2. Electrolyte rebalancing

Remixing is the most commonly used method developed to rebalance the electrolyte. A complete remix, achieved by draining all the anolyte and catholyte, mixing them together, and splitting and reloading into the tanks, is time and labour-consuming. As such, a physical partial remix approach was developed. Luo et al. [170] performed a physical partial remix of the electrolyte after 200 cycles. By measuring the concentration and oxidation state of the anolyte and catholyte, the amount of electrolyte for remixing can be determined. Rudolph et al. [176] performed remixing on a discharged battery, where a small volume of catholyte was simply transferred into the anolyte and an equal amount of anolyte was poured into catholyte.

As physical remixing of electrolytes interrupts the VRFB operation, non-interruptive methods have also been developed. Mou et al. [177] invented a method by connecting the anolyte and catholyte tanks with a pipe to periodically rebalance the electrolyte, which can make the VRFB operate continuously for a long period of time. The ratio of pipe length and diameter is key to maintain the balance. Luo et al. [170] developed an inter-diffusion method where the surplus vanadium ions in the positive side were transferred back to the negative side.

After studying the capacity fade for mixed acid electrolyte, UET [175] found that, during long term operation, the ratio of catholyte and anolyte concentration remained constant: 1.3:1. Based on this finding, they designed an overflow system with different volume (volume ratio: 1.3:1) anolyte and catholyte tanks, in which the volume ratio and total vanadium were kept constant. With the new design, the VRFB achieved long term capacity and efficiency stability. However, this design is only valid for the mixed acid electrolyte system. Recently, Wang et al. [173] developed an electrolyte reflow method to solve the electrolyte imbalance issue for the sulfuric acid-vanadium electrolyte system. Figure 12 shows the schematic of the reflow method. Without reflow, after certain cycles, all the anolyte is moved to the catholyte tank, while with reflow the anolyte tank always contained some electrolyte. Similar to the UET method, the volume ratio of catholyte to anolyte is a key parameter affecting the capacity stability depending on the operating current density. Cycle life and total capacity were all improved with the reflow method. Shaferner et al. [178] just published a dynamic model to simulate the species crossover in a VRFB. They proposed a continuous overflow method to reduce the capacity loss, where the two electrolyte tanks were connected and continuous flow between the two tanks was allowed during the cycling. The model was validated with experimental measurements and it was found that capacity decay was significantly reduced once an optimal overflow rate (2.5 mL h^{-1}) was selected. However, electrolyte precipitation was an issue in this method

and it could not prevent capacity decay over the long term; complete remixing was needed over long term operation.

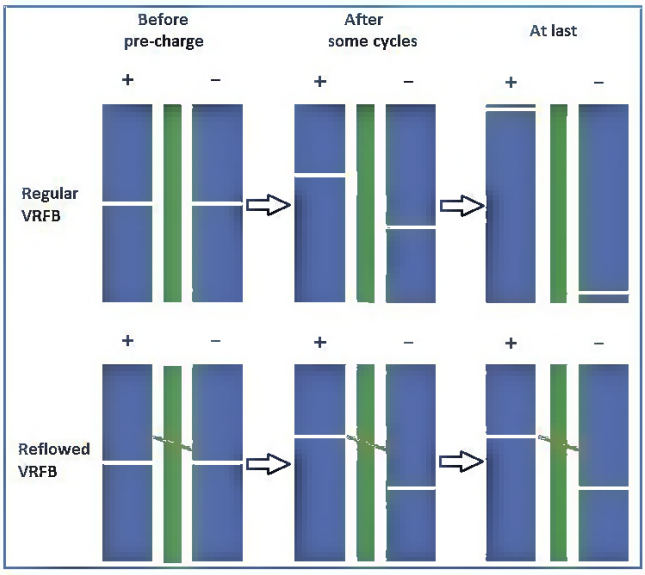

Figure 12 Schematic representation of the electrolyte-reflow method [173] (Reproduced with permission from Elsevier)

Although rebalancing electrolyte by periodical or continuous overflow from one tank to the other reduces capacity decay over long term operation, there is a trade-off between reduction of capacity decay and loss of efficiencies. Active species flowing from one side to the other can lead to the consumption of active species in both tanks, which lowers the energy efficiency. Agar et al. [179] observed the loss of efficiencies when they developed a method to reduce capacity decay by using different current at charge and discharge. It was found that capacity loss was reduced when higher current density was used in the charge process than in discharge process. It was also found that the capacity reduction effect was dependent on the membranes used and for a diffusion-dominated membrane, the capacity loss was less significant than a convection-dominated membrane. However, this technique might be impractical in real applications; in the VRFB industry, constant current operation, especially for the charging process, is not typically the method of choice, as SOC is often used to control the charge and discharge. Also high current density operation may lead to lower voltage efficiency. Currently there are no satisfactory solutions to solve the capacity decay issue without sacrificing efficiencies. Further development on this issue is still needed.

4. Aging prediction

In PEM fuel cells, accelerated stress tests (ASTs) have widely been used as evaluation tools for durability studies in an attempt to significantly reduce the experimental time. In an AST of a PEM fuel cell, different stressors/factors that significantly affect cell performance are applied to the fuel cell to observe degradation of the cell, to identify the probable degradation mechanisms, or to predict the lifetime of the fuel cell [180]. This concept should also apply to the VRFB technology.

4.1. Accelerated stress tests

Unlike the PEM fuel cells, in which ASTs are well established and systematically studied, there are no specific studies on accelerated lifetime testing for VRFBs. Satola et al. [166] have described bulk aging performed on a carbon fiber-polyethylene BP in vanadium electrolyte with 4 M H_2SO_4 at 80 °C for 100 h and on a commercial graphite-epoxy BP by treating it in vanadium electrolyte with an oxidation state of +5 at 80 °C for 7 days. This is evident that higher temperature has been used as an acceleration stressor for possible component aging in a real VRFB.

Recently, Mench's group [181] developed a cell-in series (CIS) technique for accelerated electrode degradation test. In this method, two cells were connected in series with one cell undergoing discharging and the other cell undergoing charging. During the operation, a constant SOC was maintained at a particular charge–discharge condition. Since the CIS method applied extra stress to the electrodes, it led to faster degradation of the electrode. As expected, electrode performance degradation occurred seven times faster in comparison with typical cycling tests, allowing a swift evaluation of the electrode. They concluded that both aggressively charging and discharging would result in performance loss.

The authors compared the CIS results with those under normal conditions. Figure 13 shows the polarization curve of the cells operated under normal conditions (200 mA cm^{-2} between 1.0 V and 1.65 V) before and after 6 days (54 cycles). It can be seen that, after 54 cycles, slight cell performance degradation was observed. For example, at 100 mA cm^{-2}, the charging potential increased by 5 mV (iR corrected voltage), and discharging potential decreased by 5 mV (iR corrected voltage), indicating some degradation occurred.

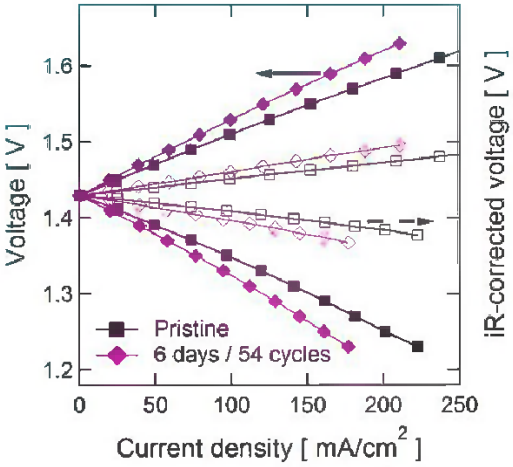

Figure 13 Polarization curves before and after 54 cycles at 200 mA cm^{-2}; solid symbols reflect uncorrected data; hollow symbols are iR-corrected; left and right axis scales are identical [181] (Reproduced with permission from ECS)

After the CIS experiments, however, significant degradation was observed. Figure 14 shows the polarization curves before and after CIS tests. After 6 days of CIS tests, the charging and discharging voltage decreased by more than 100 mV (iR corrected voltage) at 100 mA cm^{-2}, a significant degradation compared with normal cycling or even compared with electrodes soaked in 100% SOC solutions. These results indicate that the CIS method is more detrimental to the electrode than normal cycling, and that simply soaking the electrode in V(V) solution is not a stressor for electrode degradation.

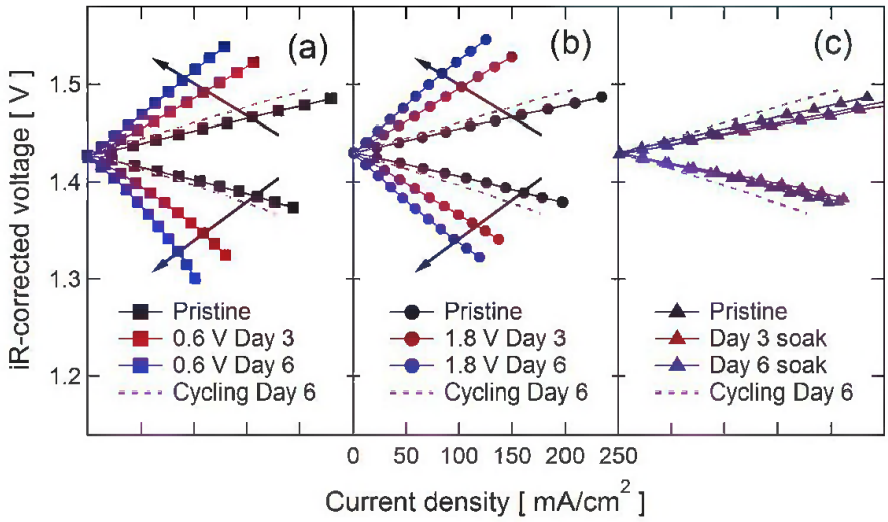

Figure 14 iR-corrected polarization curves taken after initial build, 3 d, and 6 d: (a) cell-in-series experiment E: potential hold at 0.6 V and at low SOC; (b) cell-in-series experiment F: potential hold at 1.8 V and at high SOC; and (c) soaked in high SOC solution; curve for cell cycled for 6 d shown for reference [181] (Reproduced with permission from ECS)

The fast degradation in the CIS method might be explained by the increased C=O bonding induced by high SOC [181]. As we know, oxygen content in the carbon electrode is considered an important factor affecting the VRFB performance. It was previously considered that more O content resulted in high VRFB performance [36]. However, recently Estevez et al. [140] found that only oxygen in O-C=O can enhance VRFB performance, while O-C and O=C are detrimental to the VRFB performance. In the CIS method, XPS analysis shows that SOC is the dominant factor affecting the oxygen content in the positive electrode, thus, causing a fast degradation of the electrode.

4.2. Models for aging prediction

Aging prediction is essential to estimate the overall lifetime and the cost of a battery system. Several models for vanadium redox batteries have been described, however, these models rarely focus on aging prediction, or they are not adequate for aging prediction.

Merei et al. [182] presented a multi-physics model which intended to determine all parameters that are essential for an aging prediction, including the battery's SOC, the stack and tank temperature, the corrosion current, and the V(IV) and V(V) concentrations in the reservoirs. This model combines the existing temperature model, electrochemical model, and mechanical model: the temperature model takes into account the temperature changes in the VRFB during charging and discharging; the electrochemical model considers the main electrochemical reactions and the side reactions including H_2 evolution, O_2 evolution, and vanadium diffusion through the membrane; and the mechanical model scrutinizes the pump losses within the VRFB system. Along with the existing models, this multi-physics model also considers the battery's design, electrolyte compositions, voltage, SOC, ambient temperature, and the battery system power. Through simulation, the presented model shows consistency with current experimental results. Nonetheless, the presented model still needs to be further improved.

5. Concluding remarks

As VRFBs are considered durable systems with an expected lifetime of over ten years and a cycle life of several thousand cycles, so far degradation mechanisms of the system components are scattered or scarcely addressed. This review introduces individual components of a VRFB and examines various degradation mechanisms at both cell and component levels. Based on the existing literature, major performance losses can be categorized into degradations of the electrolyte, electrode, membrane, and BP due to cross-over, side reactions, or other reasons. Following the degradation mechanisms, diagnostic tools to detect degradation mechanisms and applicable mitigation strategies for alleviating degradation are compiled for VRFB components and cells.

At this point, the main research trend in the VRFB technology is still to improve its performance and reduce its cost by developing novel materials or optimizing cell design. For example, novel membrane materials are under development although low cost perfluorinated membranes with excellent long-term stability are now being commercially manufactured; exploration of low cost electrode materials with high performance and high power density have become one of the hot spots in the development of the technology; and cell architecture/design is being improved to enhance system performance and efficiency.

Degradation of the VRFB system and its components has attracted less attention. Communication with the VRFB industry reveals that degradation of the VRFB system under normal lifetime testing is slow, as the materials used in VRFBs are relatively stable. This indicates that lifetime testing of the VRFB system is extremely time-consuming, which significantly delays the evaluation of novel materials. Unfortunately, accelerated lifetime testing is not on the agenda and standard protocols and tools for the evaluation of VRFB components are not yet available. The industrial development of prototypes and systems seems to have outpaced the fundamental research. Industry demands for accelerated lifetime testing and standard VRFB component evaluation protocols and tools are urgently needed. Also, fundamental understanding of the VRFB component and in-depth investigation of the degradation mechanisms are required through combined experimental and computational modeling. We believe that performance degradation of VRFB components, diagnostic tools for VRFB cell/component degradation, and accelerated lifetime testing protocols are the areas that can and should be focused on in the near future.

As for component degradation, different failure modes of material degradation will likely be associated with cell performance loss. To promote longevity, an in-depth investigation that includes all aspects of material selection along with the effects of the flowing electrolyte on overall battery performance degradation is needed. Specific areas may include: 1) a detailed evaluation of electrolyte impurity effects on cell performance degradation; 2) further studies to reduce gassing side reactions; 3) component stability at higher potential and long-term cycling; 4) a better understanding of the electrode/electrolyte interface and micro/nano structure on VRFB degradation; and 5) an investigation of more effective mitigation strategies to enhance component stability over a wider operating range.

Throughout the review we have shed light on VRFB components and their degradation mechanisms, compiled available diagnostic tools, and accumulated mitigation strategies for component and cell degradation, all of which help gain a systematic understanding of VRFB durability and degradation. In particular, future research directions identified within will further enhance the development of the technology in finding solutions to existing degradation issues, leading to further technology penetration of the market.

Acknowledgements

This work is financially supported by the National Research Council of Canada’s Program of Energy Storage for Grid Security and Modernization.

References

[1]. A. Z. Weber, M. M. Mench, J. P. Meyers, P. N. Ross, J. T. Gostick, Q. Liu, Redox flow batteries: a review, J. Appl. Electrochem. 41 (2011) 1137-1164.

[2]. M. Baumann, B. Zimmermann, H. Dura, B. Simon, M. Weil, A comparative probabilistic economic analysis of selected stationary battery systems for grid applications, 4th International Conference on Clean Electrical Power: Renewable Energy Resources Impact, ICCEP 2013/IEEE Article number 6586972 (2013) 87-92

[3]. M. Skyllas-Kazacos, M. H. Chakrabarti, S. A. Hajimolana, F. S. Mjalli, and M. Saleem, Progress in flow battery research and development, J. Electrochem. Soc. 158 (2011) R55-R79.

[4]. M. Bartolozzi, Development of redox flow batteries. A historical bibliography, J. Power Sources 27 (1989) 219-234.

[5]. J. Giner, L. Swette, H. Cahill, Screening of redox couples and electrode materials, Final report prepared for NASA-Lewis Research Center under Contract Number NAS3-19760 (1976) 1-108.

[6]. L. H. Thaller, Recent advances in redox flow cell storage systems, Technical Memorandum supported by DOE, DOE/NASA/1 002-79/4, NASA TM-79186 (1979) 1-11.

[7]. C. Song, H. Wang, A. Platt, H. Li, Development of diagnostic tools and accelerated testing protocols for redox flow batteries - Literature review on vanadium redox flow battery degradation, NRC report, NRC-EME-55863 (2017) 1-65.

[8]. National Aeronautics and Space Administration Lewis Research Center, Redox flow cell development and demonstration project – Calendar year 1976, Technical Memorandum supported by DOE, NASA TM-73873 (1977) 1-52.

[9]. A. Price, S. Bartley, S. Male, G. Cooley, Novel approach to utility scale energy storage, Power Eng. J. 13 (1999) 122-129.

[10]. M. A. Green, M. Rychcik, R. G. Robins, A. G. Fane, New all-vanadium redox flow cell, J. Electrochem. Soc. 133 (1986) 1057-1058.

[11]. M. Skyllas-Kazacos, Novel vanadium chloride/polyhalide redox flow battery, J. Power Sources 124 (2003) 299-302.

[12]. K. J. Cathro, K. Cedzynska, D. C. Constable, Preparation and performance of plastic-bonded-carbon bromine electrodes, J. Power Sources 19 (1987) 337-356

[13]. Y. Chiang, W. C. Carter, B. Ho, M. Duduta, High energy density redox flow device, WO Patent WO/2009/151639 (2009) 1-31.

[14]. M. Duduta, B. Ho, V. C. Wood, P. Limthongkul, V. E. Brunini, W. Craig Carter, Y. M. Chiang, Semi-solid lithium rechargeable flow battery, Adv. Energy Mater. 1 (2011) 511-516.

[15]. M. Ulaganathan, V. Aravindan, Q. Yan, S. Madhavi, M. Skyllas-Kazacos, T. M. Lim, Recent advancements in all-vanadium redox flow batteries, Adv. Mater. Interfaces, Article number 1500309, 3 (2016) 1-22.

[16]. J. Noack, N. Roznyatovskaya, T. Herr, P. Fischer, The chemistry of redox-flow batteries, Angew. Chem. 127 (2015) 9912-9947.

[17]. G. L. Soloveichik, Flow batteries: current status and trends, Chem. Rev. 115 (2015) 11533−11558.

[18]. W. Wang, Q. Luo, B. Li, X. Wei, L. Li, Z. Yang, Recent progress in redox flow battery research and development, Adv. Funct. Mater. 23 (2013) 970-986.

[19]. P. Leung, X. Li, C. Ponce de León, L. Berlouis, C. T. J. Low, F. C. Walsh, Progress in redox flow batteries, remaining challenges and their applications in energy storage, RSC Advances, 2 (2012) 10125-10156.

[20]. P. Alotto, M. Guarnieri, F. Moro, Redox flow batteries for the storage of renewable energy: A review, Renew. Sust. Energ. Rev. 29 (2014) 325-335.

[21]. C. Ding, H. Zhang, X. Li, T. Liu, F. Xing, Vanadium flow battery for energy storage: prospects and challenges, J. Phys. Chem. Lett. 4 (2013) 1281−1294.

[22]. C. Blanc, A. Rufer, Chapter 18 Understanding the vanadium redox flow batteries in Paths to Sustainable Energy, edited by A. Ng, ISBN 978-953-307-401-6 (664 pages), InTech (2010) 333-358.

[23]. C. Yin, S. Guo, H. Fang, J. Liu, Y. Li, H. Tang, Numerical and experimental studies of stack shunt current for vanadium redox flow battery, Appl. Energy 151 (2015) 237-248.

[24]. K. W. Knehr, E. C. Kumbur, Open circuit voltage of vanadium redox flow batteries: Discrepancy between models and experiments, Electrochem. Commun. 13 (2011) 342-345.

[25]. M. Pavelka, F. Wandschneider, P. Mazur, Thermodynamic derivation of open circuit voltage in vanadium redox flow batteries, J. Power Sources, 293 (2015) 400-408.

[26]. A. A. Shah, H. Al-Fetlawi, F. C. Walsh, Dynamic modelling of hydrogen evolution effects in the all-vanadium redox flow battery, Electrochim. Acta 55 (2010) 1125-1139.

[27]. H. Al-Fetlawi, A. A. Shah, F. C. Walsh, Modelling the effects of oxygen evolution in the all-vanadium redox flow battery, Electrochim. Acta 55 (2010) 3192-3205.

[28]. E. Sum, M. Skyllas-Kazacos, A study of the V(II)/V(III) redox couple for redox flow cell applications, J. Power Sources 15 (1985) 179-190.

[29]. E. Sum, M. Rychcik, M. Skyllas-Kazacos, Investigation of the V(V)/V(IV) system for use in the positive half- cell of a redox battery, J. Power Sources 16 (1985) 85-95.

[30]. G. Kear, A. A. Shah, F. C. Walsh, Development of the all-vanadium redox flow battery for energy storage: a review of technological, financial and policy aspects, Int. J. Energy Res. 36 (2012) 1105-1120.

[31]. L. Grande, Redox flow batteries 2017-2027: Markets, trends, applications, https://www.prnewswire.com/news-releases/redox-flow-batteries-2017-2027-markets-trends-applications-300527996.html, accessed on Nov. 26, 2018.

[32]. https://spectrum.ieee.org/green-tech/fuel-cells/its-big-and-longlived-and-it-wont-catch-fire-the-vanadium-redoxflow-battery, accessed on Nov. 29, 2018.

[33]. M. Skyllas-Kazakos, L. Cao, M. Kazakos, N. Kausar, A. Mousa, Vanadium electrolyte studies for the vanadium redox battery – A review, ChemSusChem 9 (2016) 1521-1543.

[34]. Á. Cunha, J. Martins, N. Rodrigues, F. P. Brito, Vanadium redox flow batteries: a technology review, Int. J. Energy Res. 39 (2015) 889-918.

[35]. C. Choi, S. Kim, R. Kim, Y. Choi, S. Kim, H.-Y. Jung, J. H. Yang, H.-T. Kim, A review of vanadium electrolytes for vanadium redox flow batteries, Renewable and Sustainable Energy Rev. 69 (2017) 263-274.

[36]. K. J. Kim, M.-S. Park, Y.-J. Kim, J. H. Kim, S. X. Dou, M. Skyllas-Kazacos, A technology review of electrodes and reaction mechanisms in vanadium redox flow batteries, J. Mater. Chem. A, 3 (2015) 16913-16933.

[37]. B. Schwenzer, J. Zhang, S. Kim, L. Li, J. Liu, Z. Yang, Membrane development for vanadium redox flow batteries, ChemSusChem 4 (2011) 1388-1406.

[38]. T. N. L. Doan, T. K. A. Hoang, P. Chen, Recent development of polymer membranes as separators for all-vanadium redox flow batteries, RSC Adv., 5 (2015) 72805-72815.

[39]. X. Li, H. Zhang, Z. Mai, H. Zhang, I. Vankelecom, Ion exchange membranes for vanadium redox flow battery (VRB) applications, Energy Environ. Sci., 4 (2011) 1147-1160.

[40]. N. Tokudu, T. Kanno, T. Hara, T. Shigematsu, Y. Tsutsui, A. Ikeuchi, T. Itou, T. Kumamoto, Development of a redox flow battery system, SEI Tech. Rev., 50 (2000) 88-94.

[41]. S. Kim, M. Vijayakumar, W. Wang, J. L. Zhang, B. W. Chen, Z. M. Nie, F. Chen, J. Z. Hu, L. Y. Li, Z. G. Yang, Chloride supporting electrolytes for all-vanadium redox flow batteries. Phys. Chem. Chem. Phys. 13 (2011) 18186−18193.

[42]. B. Li, Z. Xie, W. Jin, H. Ma, Study on Partial degradation operation modes of VRB-ESS, Adv. Mater. Res. 512-515 (2012) 1074-1078.

[43]. J. Noack, L. Vorhauser, K. Pinkwart, J. Tuebke, Aging studies of vanadium redox flow batteries, ECS Transactions, 33 (2011) 3-9.

[44]. M. Skyllas-Kazacos, C. Menictas, M. Kazacos, Thermal stability of concentrated V(V) electrolytes in the vanadium rcdox Cell, J. Electrochem. Soc.143 (1996) L86-L88.

[45]. F. Rahman, M. Skyllas-Kazacos, Solubility of vanadyl sulfate in concentrated sulfuric acid solutions, J. Power Sources 72 (1998) 105-110.

[46]. M. Kazacos, M. Cheng, M. Skyllas-Kazacos, Vanadium redox cell electrolyte optimization studies, J. Appl. Electrochem. 20 (1990) 463-467.

[47]. F. Rahman, M. Skyllas-Kazacos, Vanadium redox battery: Positive half-cell electrolyte studies, J. Power Sources 189 (2009) 1212-1219.

[48]. M. Kazakos, M. Skyllas-Kazacos, High energy density vanadium electrolyte solutions, methods of preparation thereof an all-vanadium redox cells and batteries containing high energy vanadium electrolyte solutions, WO9635239A1 (1996).

[49]. N. Kausar, R. Howe, M. Skyllas-Kazacos, Raman spectroscopy studies of concentrated vanadium redox battery positive electrolytes, J. Appl. Electrochem. 31 (2001) 1327-1332.

[50]. M. Skyllas-Kazacos, C. Peng, M. Cheng, Evaluation of precipitation inhibitors for supersaturated vanadyl electrolytes for the vanadium redox flow battery, Electrochem. Solid-State Lett. 2 (1999) 121-122.

[51]. M. Vijayakumar, L. Li, G. Graff, J. Liu, H. Zhang, Z. Yang, J. Z. Hu, Towards understanding the poor thermal stability of V^{5+} electrolyte solution in vanadium redox flow batteries, J. Power Sources 196 (2011) 3669-3672.

[52]. J. X. Zhao, Z. H. Wu, J. Y. Xi, X. P. Qiu, Solubility rules of negative electrolyte $V_2(SO_4)_3$ of vanadium redox flow battery, J. Inorg. Mater. 27 (2012) 469-474.

[53]. S. Xiao, L. Yu, L. Wu, L. Liu, X. Qiu, J. Xi, Broad temperature adaptability of vanadium redox flow battery – Part 1: electrolyte research, Electrochim. Acta 187 (2016) 525-534.

[54]. L. Cao , M. Skyllas-Kazacos, C. Menictas, J. Noack, A review of electrolyte additives and impurities in vanadium redox flow batteries, J. Energy Chem., article in press, 2018

[55]. M. Kubata, H. Nakaishi, N. Tokuda, Electrolyte for redox flow battery, and redox flow battery, US7258947B2 (2007).

[56]. A. W. Burch, Impurity effects in all-vanadium redox flow batteries, Master's Thesis, University of Tennessee (2015).

[57]. J. H. Park, J. J. Park, H. J. Lee, B. S. Min, and J. H. Yang, Influence of metal impurities or additives in the electrolyte of a vanadium redox flow battery, J. Electrochem. Soc., 165 (2018) A1263-A1268.

[58]. M. Kazacos, Electrolyte optimization and electrode material evaluation for the vanadium redox battery, MSc Thesis, University of New South Wales, Australia (1989). http://unsworks.unsw.edu.au/fapi/datastream/unsworks:40475/SOURCE01?view=true

[59]. N. Kausar, Studies of V(IV) and V(V) species in vanadium cell electrolyte, PhD Thesis, University of New South Wales, Australia (2002). http://unsworks.unsw.edu.au/fapi/datastream/unsworks:36347/SOURCE01?view=true.

[60]. A. Mousa, Chemical and electrochemical studies of V(III) and V(II) solutions in sulfuric acid solution for vanadium battery applications, PhD Thesis, University of New South Wales , Australia, (2003). http://unsworks.unsw.edu.au/fapi/datastream/unsworks:36320/SOURCE01?view=true

[61]. H. J. Lee, N. H. Choi, H. Kim, Analysis of concentration polarization using UV-Visible spectrophotometry in a vanadium redox flow battery, J. Electrochem. Soc. 161 (2014) A1291-A1296.

[62]. R. P. Brooker, C. J. Bell, L. J. Bonville, H. R. Kunz, J. M. Fenton, Determining vanadium concentrations using the UV-Vis response method, J. Electrochem. Soc. 162 (2015) A608-A613.

[63]. M. Skyllas-Kazacos, M. Kazacos, State of charge monitoring methods for vanadium redox flow battery control, J Power Sources 196 (2011) 8822-8827.

[64]. N. H. Choi, S.-K. Kwon, H. Kim, Analysis of the oxidation of the V(II) by dissolved oxygen using UV-visible spectrophotometry in a vanadium redox flow battery, J. Electrochem. Soc. 160 (2013) A973-A979.

[65]. M. Vijayakumar, S. D. Burton, C. Huang, L. Li, Z. Yang, G. L. Graff et al. Nuclear magnetic resonance studies on vanadium(IV) electrolyte solutions for vanadium redox flow battery, J. Power Sources 195 (2010) 7709-7717.

[66]. W. P. Griffith, P. J. B. Lesniak, Raman studies on species in aqueous solutions. Part III. Vanadates, molybdates, and tungstates, J. Chem. Soc. A (1969) 1066-1071.

[67]. W. P. Griffith, T. D. Wickins, Raman studies on species in aqueous solutions. Part II. Oxy-species of metals of Groups VIA, VA, and IVA, J. Chem. Soc. A (1967) 675-679.

[68]. W. P. Griffith, T. D. Wickins, Raman studies on species in aqueous solutions. Part I. The vanadates, J. Chem. Soc. A (1966) 1087-1090.

[69]. C. Madic, G. M. Begun, R. L. Hahn, J. P. Launay, W. E. Thiessen, Raman spectroscopy of neptunyl and plutonyl ions in aqueous solution: Hydrolysis of Np(VI) and Pu(VI) and disproportionation of Pu(V), Inorg. Chem. 23 (1984) 469-476.

[70]. M. Skyllas-Kazacos, M. Kazacos, Stabilized electrolyte solutions, methods of preparation thereof and redox cells and batteries containing stabilized electrolyte solutions, Pinnacle VRB Ltd., US6143443 (2000) 1-90.

[71]. A. Mousa, M. Skyllas-Kazacos, Effect of additives on the lowtemperature stability of vanadium redox flow battery negative half-cell Electrolyte, ChemElectroChem 2 (2015) 1742-1751.

[72]. S. Roe, C. Menictas, M. Skyllas-Kazacos, A high energy density vanadium redox flow battery with 3 M vanadium electrolyte, J. Electrochem. Soc. 163 (2016) A5023-A5028.

[73]. N. Kausar, A. Mousa, M. Skyllas-Kazacos, The effect of additives on the high-temperature stability of the vanadium redox flow battery positive electrolytes, ChemElectroChem 3 (2016) 276-282.

[74]. J. G. Lee, S. J. Park, Y. I. Cho, Y. G. Shul, A novel cathodic electrolyte based on H2C2O4 for a stable vanadium redox flow battery with high charge–discharge capacities, RSC Adv. 3 (2013) 21347-21351.

[75]. M. Vijayakumar, W. Wang, Z. Nie, V. Sprenkle, J. Z. Hu, Elucidating the higher stability of vanadium(V) cations in mixed acid based redox flow battery electrolytes, J. Power Sources 241 (2013) 173-177.

[76]. G. Wang, J. Chen, X. Wang, J. Tian, H. Kang, X. Zhu, Y. Zhang, X. Liu, R. Wang, Influence of several additives on stability and electrochemical behavior of V(V) electrolyte for vanadium redox flow battery, J. Electroanal. Chem. 709 (2013) 31-38.

[77]. C. Ding, X. Ni, X. Li, X. Xi, X. Han, X. Bao, H. Zhang, Effects of phosphate additives on the stability of positive electrolytes for vanadium flow batteries, Electrochim. Acta 164 (2015) 307-314.

[78]. H. Prifti, A. Parasuraman, S. Winardi, T. M. Lim, M. Skyllas-Kazacos, Membranes for redox flow battery applications, Membranes, 2 (2012) 275-306.

[79]. S.-H. Cha, Recent development of nanocomposite membranes for vanadium redox flow batteries, J. Nanomater. Article ID 207525 (2015) 1-12.

[80]. Q. T. Luo, H. M. Zhang, J. Chen, P. Qian, Y. F. Zhai, Modification of nafion membrane using interfacial polymerization for vanadium redox flow battery applications. J. Membrane Sci. 311 (2008) 98-103.

[81]. J. Xi, Z. Wu, X. Teng, Y. Zhao, L. Chen, X. Qiu, Self-assembled polyelectrolyte multilayer modified nafion membrane with suppressed vanadium ion crossover for vanadium redox flow batteries. J. Mater. Chem. 18 (2008) 1232-1238.

[82]. Z. Mai, H. Zhang, X. Li, S. Xiao, Nafion/polyvinylidene fluoride blend membranes with improved ion selectivity for vanadium redox flow battery application. J. Power Sources 196 (2011) 5737-5741.

[83]. C. Fujimoto, S. Kim, R. Stains, X. Wei, L. Li, Z. G. Yang, Vanadium redox flow battery efficiency and durability studies of sulfonated Diels Alder poly(phenylene)s, Electrochem. Commun. 20 (2012) 48-51.

[84]. H.-S. Choi, Y.-H. Oh, C.-H. Ryu, G.-J. Hwang, Characteristics of the all-vanadium redox flow battery using anion exchange membrane, J. Taiwan Inst. Chem. Eng. 45 (2014) 2920-2925.

[85]. D.-H. Kim, J.-S. Park, M. Choun, J. Lee, M.-S. Kang, Pore-filled anion-exchange membranes for electrochemical energy conversion applications, Electrochim. Acta 222 (2016) 212-220.

[86]. M. S. Lee, H. G. Kang, J. D. Jeon, Y. W. Choi, Y. G. Yoon, Novel amphoteric ion-exchange membrane prepared by the pore-filling technique for vanadium redox flow batteries, RSC Adv. 6 (2016) 63023-63029.

[87]. Y. Wang, S. Wang, M. Xiao, S. Song, D. Han, M. A. Hickner, Y. Meng, Amphoteric ion exchange membrane synthesized by direct polymerization for vanadium redox flow battery application, Int. J. Hydrogen Energy 39 (2014) 16123-16131.

[88]. G. Hu, Y. Wang, J. Ma, J. Qiu, J. Peng, J. Li, M. Zhai, A novel amphoteric ion exchange membrane synthesized by radiation-induced grafting α-methylstyrene and N,N-dimethylaminoethyl methacrylate for vanadium redox flow battery application, J. Membr. Sci. 407-408 (2012) 184-192.

[89]. X. Wei, B. Li, W. Wang, Porous polymeric composite separators for redox flow batteries, Polym. Rev. 55 (2015) 247-272.

[90]. B. Tian, C. W. Yan, F. H. Wang, Proton conducting composite membrane from Daramic/Nafion for vanadium redox flow battery. J. Membr. Sci. 234 (2004) 51-54.

[91]. S. C. Chieng, M. Kazacos, M. Skyllas-Kazacos, Modification of Daramic, microporous separator, for redox flow battery applications, J. Membr. Sci. 75 (1992) 81-91.

[92]. X. Wei, Z. Nie, Q. Luo, B. Li, V. Sprenkle, Wei Wang, Polyvinyl chloride/silica nanoporous composite separator for all-vanadium redox flow battery applications, J. Electrochem. Soc. 160 (2013) A1215-A1218.

[93]. E. Agar, K. W. Knehr, D. Chen, M. A. Hickner, E. C. Kumbur, Species transport mechanisms governing capacity loss in vanadium flow batteries: Comparing Nafion® and sulfonated Radel membranes, Electrochim. Acta 98 (2013) 66-74.

[94]. J. Sun, D. Shi, H. Zhong, X. Li, H. Zhang, Investigations on the self-discharge process in vanadium flow battery, J. Power Sources 294 (2015) 562-568.

[95]. C. Sun, J. Chen, H. Zhang, X. Han, Q. Luo, Investigations on transfer of water and vanadium ions across Nafion membrane in an operating vanadium redox flow battery, J. Power Sources 195 (2010) 890-897.

[96]. J. Sun, X. Li, X. Xi, Q. Lai, T. Liu, H. Zhang, The transfer behavior of different ions across anion and cation exchange membranes under vanadium flow battery medium, J. Power Sources 271 (2014) 1-7.

[97]. B. Li, Q. Luo, X. Wei, Z. Nie, E. Thomsen, B. Chen, V. Sprenkle, W. Wang, Capacity decay mechanism of microporous separator-based all-vanadium redox flow batteries and its recovery, ChemSusChem 7 (2014) 577-584.

[98]. M. Skyllas-Kazacos, L. Goh, Modeling of vanadium ion diffusion across the ion exchange membrane in the vanadium redox battery, J. Membr. Sci. 399-400 (2012) 43-48.

[99]. R. A. Elgammal, Z. Tang, C.-N. Sun, J. Lawton, T. A. Zawodzinski Jr., Species uptake and mass transport in membranes for vanadium redox flow batteries, Electrochim. Acta 237 (2017) 1-11.

[100]. T. Sukkar, M. Skyllas-Kazacos, Water transfer behaviour across cation exchange membranes in the vanadium redox battery, J. Membr. Sci. 222 (2003) 235-247.

[101]. T. Mohammadi, S. C. Chieng, M. Skyllas-Kazacos, Water transport study across commercial ion exchange membranes in the vanadium redox flow battery, J. Membr. Sci. 133 (1997) 151-159.

[102]. T. Sukkar, M. Skyllas-Kazacos, Membrane stability studies for vanadium redox cell applications, J. Appl. Electrochem. 34 (2004) 137-145.

[103]. S. Kim, T. B. Tighe, B. Schwenzer, J. Yan, J. Zhang, J. Liu, Z. Yang, M. A. Hickner, Chemical and mechanical degradation of sulfonated poly(sulfone) membranes in vanadium redox flow batteries, J. Appl. Electrochem., 41 (2011) 1201-1213.

[104]. X. Huang, Y. Pu, Y. Zhou, Y. Zhang, H. Zhang, In-situ and ex-situ degradation of sulfonated polyimide membrane for vanadium redox flow battery application, J. Membr. Sci. 526 (2017) 281-292.

[105]. D. Chen and M. A. Hickner, V^{5+} degradation of sulfonated Radel membranes for vanadium redox flow batteries, Phys. Chem. Chem. Phys. 15 (2013) 11299-11305

[106]. T. Mohammadi, M. Skyllas Kazacos, Evaluation of the chemical stability of some membranes in vanadium solution, J. Appl. Electrochem. 27 (1997) 153-160.

[107]. E. Wiedemann, A. Heintz, R. N. Lichtenthaler, Transport properties of vanadium ions in cation exchange membranes: Determination of diffusion coefficients using a dialysis cell, J. Membr. Sci. 141 (1998) 215-221.

[108]. A. Heintz, E. Wiedemann, J. Ziegler, Ion exchange diffusion in electromembranes and its description using the Maxwell-Stefan formalism, J. Membr. Sci. 137 (1997) 121-132.

[109]. S. C. Chieng, Membrane processes and membrane modification for redox flow battery applications, PhD thesis, University of New South Wales: Sydney, Australia, (1993).

[110]. D. Chen, S. Wang, M. Xiao, Y. Meng, Preparation and properties of sulfonated poly(fluorenyl ether ketone) membrane for vanadium redox flow battery application, J. Power Sources, 195 (2010) 2089-2095.

[111]. J. Fang, H. Xu, X. Wei, M. Guo, X. Lu, C. Lan, Y. Zhang, Y. Liu and T. Peng, Preparation and characterization of quaternized poly (2,2,2-trifluoroethyl methacrylate-co-N-vinylimidazole) membrane for vanadium redox flow battery, Polym. Adv. Technol. 24 (2013) 168-173.

[112]. W. Wei, H. Zhang, X. Li, H. Zhang, Y. Li, I. Vankelecom, Hydrophobic asymmetric ultrafiltration PVDF membranes: an alternative separator for VFB with excellent stability, Phys. Chem. Chem. Phys. 15 (2013) 1766-1771.

[113]. X. Luo, Z. Lu, J. Xi, Z. Wu, W. Zhu, L. Chen, X. Qiu, Influences of permeation of vanadium ions through PVDF-g-PSSA membranes on performances of vanadium redox flow batteries, J. Phys. Chem. B 109 (2005) 20310-20314.

[114]. J. Qiu, L. Zhao, M. Zhai, J. Ni, H. Zhou, J. Peng, J. Li, G. Wei, Pre-irradiation grafting of styrene and maleic anhydride onto PVDF membrane and subsequent sulfonation for application in vanadium redox batteries, J. Power Sources 177 (2008) 617-623.

[115]. C. Fujimoto, Advanced membranes for vanadium redox flow batteries (VRFB), DOE Energy Storage Annual Review Meeting, Washington DC, USA, Sept. 26-28, 2016

[116]. X. L. Zhou, T. S. Zhao, L. An, L. Wei, C. Zhang, The use of polybenzimidazole membranes in vanadium redox flow batteries leading to increased coulombic efficiency and cycling performance, Electrochim. Acta 153 (2015) 492-498.

[117]. L. Zeng, T. S. Zhao, L. Wei, Y. K. Zeng, Z. H. Zhang, Highly stable pyridinium-functionalized cross-linked anion exchange membranes for all vanadium redox flow batteries, J. Power Sources 331 (2016) 452-461.

[118]. D. Chen, M. A. Hickner, E. Agar, E. C. Kumbur, Optimizing membrane thickness for vanadium redox flow batteries, J. Membr. Sci. 437 (2013) 108-113.

[119]. I. Derr, M. Bruns, J. Langner, A. Fetyan, J. Melke, C. Roth, Degradation of all-vanadium redox flow batteries (VRFB) investigated by electrochemical impedance and X-ray photoelectron spectroscopy: Part 2 electrochemical degradation, J. Power Sources 325 (2016) 351-359.

[120]. I. Derr, Electrochemical degradation and chemical aging of carbon felt electrodes in all-vanadium redox flow batteries, Doctor thesis, Department of Biology, Chemistry and Pharmacy of Freie Universität Berlin, Berlin, 2017

[121]. A. Parasuraman, T. M. Lima, C. Menictas, M. Skyllas-Kazacos, Review of material research and development for vanadium redox flow battery applications, Electrochim. Acta 101 (2013) 27-40.

[122]. M. H. Chakrabarti, N. P. Brandon, S. A. Hajimolana, F. Tariq, V. Yufit, M. A. Hashim, M. A. Hussain, C. T. J. Low, P. V. Aravin, Application of carbon materials in redox flow batteries, J. Power Sources 253 (2014) 150-166.

[123]. I. Derr, A. Fetyan, K. Schutjajew, C. Roth, Electrochemical analysis of the performance loss in all vanadium redox flow batteries using different cut-off voltages, Electrochim. Acta 224 (2017) 9-16.

[124]. I. Derr, D. Przyrembel, J. Schweer, A. Fetyan, J. Langner, J. Melke, M. Weinelt, C. Roth, Electroless chemical aging of carbon felt electrodes for the all-vanadium redox flow battery (VRFB) investigated by Electrochemical Impedance and X-ray Photoelectron Spectroscopy, Electrochim. Acta 246 (2017) 783-793.

[125]. H. Liu, Q. Xu, C. Yan, Y. Qiao, Corrosion behavior of a positive graphite electrode in vanadium redox flow battery, Electrochim. Acta 56 (2011) 8783-8790.

[126]. H. Liu, Q. Xu, C. Yan, On-line mass spectrometry study of electrochemical corrosion of the graphite electrode for vanadium redox flow battery, Electrochem. Commun. 28 (2013) 58-62.

[127]. X. Wu, H. Xu, Y. Shen, P. Xu, L. Lu, J. Fu, H. Zhao, Treatment of graphite felt by modified Hummers method for the positive electrode of vanadium redox flow battery, Electrochim. Acta 138 (2014) 264-269.

[128]. C.-N. Sun, F. M. Delnick, D. S. Aaron, A. B. Papandrew, M. M. Mench, T. A. Zawodzinski Jr, Resolving losses at the negative electrode in all-vanadium redox flow batteries using electrochemical impedance spectroscopy, J. Electrochem. Soc. 161 (2014) A981-A988.

[129]. V. Haddadi-Asl, M. S. Rabbani, Effect of electrochemical cell overcharge on electrical and electrochemical properties of polymer composite electrodes (II): Mechanism of electrode deterioration, Iran. Polym. J. 7 (1998) 185-194.

[130]. F. Mohammadi, P. Timbrell, S. Zhong, C. Padeste, M. Skyllas-Kazacos, Overcharge in the vanadium redox battery and changes in electrical resistivity and surface functionality of graphite-felt electrodes, J. Power Sources 52 (1994) 61-68.

[131]. A. Di Blasi, O. Di Blasi, N. Briguglio, A. S. Aricò, D. Sebastián, M. J. Lázaro, G. Monforte, V. Antonucci, Investigation of several graphite-based electrodes for vanadium redox flow cell, J. Power Sources 227 (2013) 15-23.

[132]. P. Trogadas, O. O. Taiwo, B. Tjaden, T. P. Neville, S. Yun, J. Parrondo, V. Ramani, M.-O. Coppens, D. J. L. Brett, P. R. Shearing, X-ray micro-tomography as a diagnostic tool for the electrode degradation in vanadium redox flow batteries, Electrochem. Commun. 48 (2014) 155-159.

[133]. X. Li, K. Huang, Q. Liu, N. Tan, L. Chen, Characteristics of graphite felt electrode electrochemically oxidized for vanadium redox battery application, Trans. Nonferrous Met. Soc. China 17 (2007), 195-199.

[134]. C. Song, R. Hui, J. Zhang, High temperature PEM fuel cell catalysts and catalyst layers, in J. Zhang ed. PEM fuel cell electrocatalysts and catalyst layers, Springer, 2008

[135]. P. Mazúra, J. Mrlík, J. Beneš, J. Pocedič, J. Vrána, J. Dundálek, J. Kosek, Performance evaluation of thermally treated graphite felt electrodes for vanadium redox flow battery and their four-point single cell characterization, J. Power Sources 380 (2018) 105-114.

[136]. G. Wei, X. Fan, J. Liu, C. Yan, A review of the electrochemical activity of carbon materials in vanadium redox flow batteries, New Carbon Mater. 29 (2014) 272-279.

[137]. L. Shi, S. Liu, Z. He, J. Shen, Nitrogen-Doped Graphene: Effects of nitrogen species on the properties of the vanadium redox flow battery, Electrochim. Acta 138 (2014) 93-100.

[138]. Y. Huang, Q. Deng, X. Wu, S. Wang, N, O Co-doped carbon felt for high-performance all vanadium redox flow battery, Int. J. Hydrogen Energy, 42 (2017) 7177-7185.

[139]. K. J. Kim, H. S. Lee, J. Kim, M.-S. Park, J. H. Kim, Y.-J. Kim, M. Skyllas-Kazacos, Superior electrocatalytic activity of a robust carbon-felt electrode with oxygen-rich phosphate groups for all-Vanadium redox flow atteries, ChemSusChem 9 (2016) 1329-1338.

[140]. L. Estevez, D. Reed, Z. Nie, A. M. Schwarz, M. I. Nandasiri, J. P. Kizewski, W. Wang, E. Thomsen, J. Liu, J.-G. Zhang, V. Sprenkle, B. Li, Tunable oxygen functional groups as electrocatalysts on graphite felt surfaces for all-vanadium flow batteries, ChemSusChem 9 (2016) 1455-1461.

[141]. L. Wei, T. S. Zhao, L. Zeng, X. L. Zhou, Y. K. Zeng, Copper nanoparticle-deposited graphite felt electrodes for all vanadium redox flow batteries, Appl. Energy 180 (2016) 386-391.

[142]. D. J. Suárez, Z. González, C. Blanco, M. Granda, R. Menéndez, R. Santamaría, Graphite felt modified with bismuth nanoparticles as negative electrode in a vanadium redox flow battery, ChemSusChem 7 (2014) 914-918.

[143]. H. Zhou, Y. Shen, J. Xi, X. Qiu, L. Chen, ZrO2‑Nanoparticle-Modified Graphite Felt: Bifunctional Effects on Vanadium Flow Batteries, ACS Appl. Mater. Interfaces 8 (2016) 15369−15378.

[144]. C. Gao, N. Wang, S. Peng, S. Liu, Y. Lei, X. Liang, S. Zeng, H. F. Zi, Influence of Fenton's reagent treatment on electrochemical properties of graphite felt for all vanadium redox flow battery, Electrochim. Acta 88 (2013) 193-202.

[145]. D. M. Kabtamu, J.-Y. Chen, Y.-C. Chang, C.-H. Wang, Water-activated graphite felt as a high-performance electrode for vanadium redox flow batteries, J. Power Sources 341 (2017) 270-279.

[146]. T. X. H. Le, M. Bechelany, M. Cretin, Carbon felt based-electrodes for energy and environmental applications: A review, Carbon 122 (2017) 564-591.

[147]. K. H. Kim, B. G. Kim, D. G. Lee, Development of carbon composite bipolar plate for vanadium redox flow battery, Compos. Struct. 109 (2014) 253-259.

[148]. S. Zhong, M. Kazacos, R. P. Burford, M. S. Kazacos, Fabrication and activation studies of conducting plastic composite electrodes for redox cells. J. Power Sources 36 (1991) 29-43.

[149]. V. Haddadi-Asl, M. Kazacos, M. S. Kazacos, Conductive carbon-polypropylene composite electrodes for vanadium redox flow battery, J. Appl. Electrochem. 25 (1995) 29-33.

[150]. S. Zhong, M. Kazacos, M. S. Kazacos, Flexible, conducting plastic electrode and process for its preparation, US Patent 5,665,212, September 9, 1997.

[151]. C. M. Hagg, M. S. Kazacos, Novel bipolar electrode for battery applications, J. Appl. Electrochem. 32 (2002) 1063-1069.

[152]. H. N. Yu, J. W. Lim, M. Kim, D. G. Lee, Plasma treatment of the carbon fiber bipolar plate for PEM fuel cell, Compos. Struct. 94 (2012) 1911-1918.

[153]. S. Rudolph, U. Schroder, I. M. Bayanov, G. Pfeiffer, Corrosion prevention of graphite collector in vanadium redox flow battery. J. Electroanal. Chem. 709 (2013) 93-98.

[154]. B. Caglar, J. Richards, P. Fischer, J. Tuebke, Conductive polymer composites and coated metals as alternative bipolar plate materials for all-vanadium redox flow batteries. Adv. Mater. Lett. 5 (2014) 299-308.

[155]. K. H. Kim, J. Choe, S. Nam, B. G. Kim, D. G. Lee, Surface crack closing method for the carbon composite bipolar plates of a redox flow battery, Compos. Struct. 119 (2015) 436-442.

[156]. J. Choe, J. W. Lim, M. Kim, J. Kim, D. G. Lee, Durability of graphite coated carbon composite bipolar plates for vanadium redox flow batteries, Compos. Struct. 134 (2015) 106-113.

[157]. H. Liu, L. Yang, Q. Xu, C. Yan, Corrosion behavior of a bipolar plate of carbon–polythene composite in a vanadium redox flow battery, RSC Adv. 5 (2015) 5928-5932.

[158]. B. Satola, C. N. Kirchner, L. Komsiyska, G. Wittstock, Chemical stability of graphite-polypropylene bipolar plates for the vanadium redox flow battery at resting state, J. Electrochem. Soc. 163 (2016) A2318-A2325.

[159]. A. Tang, J. McCann, J. Bao, M. S. Kazacos, Investigation of the effect of shunt current on battery efficiency and stack temperature in vanadium redox flow battery. J. Power Sources 242 (2013) 349-356.

[160]. R. E. White, C. W. Walton, H. S. Burney and R. N. Beaver, Predicting shunt current in stacks of bipolar plate cells. Electrochem. Sci. Technol. 133 (1986) 485-492.

[161]. F. Xing, H. Zhang, X. Ma, Shunt current loss of the vanadium redox flow battery, J. Power Sources 196 (2011) 10753-10757.

[162]. H. Fink, M. Remy, Shunt currents in vanadium flow batteries: Measurement, modelling and implications for efficiency, J. Power Sources 284 (2015) 547-553.

[163]. S. Nam, D. Lee, D. G. Lee, J. Kim, Nano carbon/fluoroelastomer composite bipolar plate for a vanadium redox flow battery (VRFB), Compos. Struct. 159 (2017) 220-227.

[164]. L. Yang, Y. Zhou, S. Wang, Y. Lin, T. Huang, A. Yu, A novel bipolar plate design for vanadium redox flow battery application, Int. J. Electrochem. Sci. 12 (2017) 7031-7038.

[165]. L. Komsiyska, A. Kwan, E. M. Hammer, M. Lewerenz, S. A. G. Barragan, Study of graphite based bipolar plate corrosion for vanadium redox flow batteries, Carolina Nunes Kirchner, June 27 2013 (Next Energy)

[166]. B. Satola, L. Komsiyska, G. Wittstock, Bulk aging of graphite-polypropylene current collectors induced by electrochemical cycling in the positive electrolyte of vanadium redox flow batteries, J. Electrochem. Soc. 164 (2017) A2566-A2572.

[167]. D. Lee, J. W. Lim, S. Nam, I. Choi, D. G. Lee, Method for exposing carbon fibers on composite bipolar plates, Compos. Struct. 134 (2015) 1-9.

[168]. C.-H. Chang, H.-W. Chou, N.-Y. Hsu and Y.-S. Chen, Development of integrally molded bipolar plates for all-vanadium redox flow batteries, Energies 9 (2016) 1-10.

[169]. A. Tang, J. Bao, M. Skyllas-Kazacos, Dynamic modelling of the effects of ion diffusion and side reactions on the capacity loss for vanadium redox flow battery, J. Power Sources 196 (2011) 10737-20747.

[170]. Q. Luo, L. Li, W. Wang, Z. Nie, X. Wei, B. Li, B. Chen, Z. Yang, and V. Sprenkle, Capacity decay and remediation of Nafion based all vanadium redox flow batteries, ChemSusChem 6 (2013) 268-274.

[171]. L. Wei, T. S. Zhao, Q. Xu, X. L. Zhou, and Z. H. Zhang, in-situ investigation of hydrogen evolution behavior in vanadium redox flow batteries, Appl. Energy 190 (2017) 1112-1118.

[172]. K. Ngamasai and A. Arpornwichanop, Analysis and measurement of the electrolyte imbalance in a vanadium redox flow battery, J. Power Sources 282 (2015) 534-543.

[173]. K. Wang, L. Liu, J. Xi, Z. Wu, X. Qiu, reduction of capacity decay in vanadium flow batteries by an electrolyte-reflow method, J. Power Sources 338 (2017) 17-25.

[174]. A. H. Whitehead, M. Harrer, Investigation of a method to hinder charge imbalance in the vanadium redox flow battery, J. Power Sources 230 (2013) 271-276.

[175]. UniEnergy Technologies, Two unique advantages of the chloride containing new generation VRFB chemistry, IFBF 2016, Karsruhe, Germany, June 6-8, 2016

[176]. S. Rudolph, U. Schroder, I. M. Baynov, On-line controlled state of charge rebalancing in vanadium redox flow battery, J. Electroanal. Chem. 703 (2013) 29-37.

[177]. L. Mou, M. Huang, A. Klassen, M. A. M. Harper, Redox flow battery and method for operating the battery continuously in a long period of time, US 2011/0300417 A1, Dec. 8, 2011

[178]. K. Schafner, M. Becker, T. Turek, Capacity balancing for vanadium redox flow batteries through electrolyte overflow, J. Appl. Electrochem. 48 (2018) 639-649.

[179]. E. Agar, A. Benjamin, C. R. Dennison, D. Chen, M. A. Hickner, E. C. Kumbur, Reducing capacity fade in vanadium redox flow batteries by altering charging and discharging currents, J. Power Sources 246 (2014) 767-774.

[180]. S. Zhang, X.-Z. Yuan, H. Wang, W. Mérida, H. Zhu, J. Shen, S. Wu, J. Zhang, A review of accelerated stress tests of MEA durability in PEM fuel cells, Int. J. Hydrogen Energy 34 (2009) 388-404.

[181]. A. M. Pezeshki, R. L. Sacci, G. M. Veith, T. A. Zawodzinski, M. M. Mench, The cell-in-series method: a technique for accelerated electrode degradation in redox flow batteries, J. Electrochem. Soc. 163 (2016) A5202-A5210.

[182]. G. Merei, S. Adler, D. Magnor, D. U. Sauer, Multi-physics Model for the Aging Prediction of a Vanadium Redox Flow Battery System, Electrochim. Acta 174 (2015) 945-954.